RIP140 inhibits glycolysis-dependent proliferation of breast cancer cells by regulating GLUT3 expression through transcriptional crosstalk between hypoxia induced factor and p53

Valentin Jacquier[1], Delphine Gitenay[1*], Samuel Fritsch[1], Sandrine Bonnet[1], Balázs Győrffy[2], Stéphan Jalaguier[1], Laetitia K. Linares[1], Vincent Cavaillès[1#§] and Catherine Teyssier[1#§]

[1]IRCM, Institut de Recherche en Cancérologie de Montpellier, INSERM U1194, Université Montpellier, Montpellier F-34298, France

[2]Department of Bioinformatics, Semmelweis University and TTK Lendület Cancer Biomarker Research Group, Budapest, Hungary

[*]present address: IRMB, University of Montpellier, INSERM, CNRS, CHU Montpellier, Montpellier, France

[#]Co-last authors

[§]Corresponding authors: catherine.teyssier@inserm.fr (C.T.); vincent.cavailles@inserm.fr (V.C.)

Abstract

Cancer cells with uncontrolled proliferation preferentially depend on glycolysis to grow, even in the presence of oxygen. The transcriptional co-regulator RIP140 represses the activity of transcription factors that drive cell proliferation and metabolism and plays a role in mammary tumorigenesis. Here we use cell proliferation and metabolic assays to demonstrate that RIP140-deficiency causes a glycolysis-dependent increase in breast tumor growth. We further demonstrate that RIP140 reduces the GLUT3 gene transcription, by inhibiting the transcriptional activity of hypoxia inducible factor HIF-2α in a p53 dependent mechanism. Interestingly, RIP140 expression was significantly associated with good prognosis only for breast cancer patients with tumors expressing low GLUT3, low HIF-2α and high p53, thus confirming the mechanism of RIP140 anti-tumor activity provided by our experimental data. Overall, our work establish RIP140 as a critical modulator of the p53/HIF cross-talk to inhibit breast cancer cell glycolysis and proliferation.

Keywords: breast cancer, cancer cell metabolism, glycolysis, GLUT3, transcription, RIP140, HIF, p53.

Introduction

In a normal resting cell, glycolysis converts glucose to pyruvate, which enters the tricarboxylic acid cycle where it becomes oxidized to generate ATP into mitochondria. In the absence of oxygen, glucose is still degraded into pyruvate, which is now converted into lactate. On switching to proliferative mode, cells increase glycolysis and reduce oxidative phosphorylation, which results in a high rate of glycolysis leading to lactate production. This metabolic switch was first described by Otto Warburg in the 20's, who observed that cancer cells prefer glycolysis to mitochondrial respiration to produce energy, even in the presence of oxygen (Hsu and Sabatini, 2008). This conversion of glucose to lactate is now established as the Warburg effect, or aerobic glycolysis. At first, Warburg hypothesized that cancer arises from impaired mitochondria. However, experimental observations of functional mitochondria in cancer cells have since refuted this hypothesis (Zong et al., 2016). In fact, increased aerobic glycolysis has been frequently verified in tumors. It is now established that cancer cells switch to glycolysis to supply their increased need for biosynthetic precursors and organic resources

to synthetize cell components (Vander Heiden et al., 2009). As glycolysis produces less ATP than oxidative phosphorylation, cancer cells compensate for this energy gap by up-regulating glucose transporters to import more glucose into the cell. Enhanced glycolysis also produces reducing equivalents and many glycolytic intermediates are diverted into the pentose phosphate pathway to produce NADPH (Metallo and Vander Heiden, 2013), allowing cancer cells to fight against reactive oxygen species and oxidative stress (Patra and Hay, 2014).

The switch to glycolysis in cancer cells is orchestrated by oncogenes and tumor suppressors (Razungles et al., 2013). Specifically, the tumor suppressor gene p53 favors oxidative phosphorylation over glycolysis, enhancing the production of reactive oxygen species, to imbalance redox status and promote cell death (Gomes et al., 2018; Humpton and Vousden, 2019). p53 directly inhibits glycolysis by blocking the expression of glucose transporters (Schwartzenberg-Bar-Yoseph et al., 2004) (Kawauchi et al., 2008). Conversely, inactivating p53 reduces oxygen dependence and allows cancer cells to grow in oxygen-limited conditions, such as hypoxia. Hypoxia induces the stability of hypoxia inducible factors, or HIFs, which have an oxygen sensitive α sub-unit (HIF-1α, HIF-2α or HIF-3α) and one stable β sub-unit (HIF-1β; also known as ARNT)(Majmundar et al., 2010). In cancer cells, HIFs antagonize p53

and stimulate glycolysis. However, the mechanisms of their direct influence on glycolysis needs further clarification (Amelio and Melino, 2015; Sermeus and Michiels, 2011).

The transcriptional coregulator RIP140 regulates the activity of various transcription factors, mainly inhibiting their transactivation ability by recruiting histone deacetylases (Augereau et al., 2006). RIP140 can also activate transcription through SP1 (Castet et al., 2006), or NF-κB (Zschiedrich et al., 2008) sites. Due to its wide interactome, RIP140 influences numerous physiological functions, such as mammary gland development, fertility and inflammation (Nautiyal, 2017). RIP140 is also a major regulator of energy homeostasis, regulating lipogenesis in the liver, lipid storage and thermogenesis in adipose tissues, mitochondrial integrity, and the formation of oxidative fibers in the muscle (Nautiyal, 2017). In normal adipocytes, RIP140 has been shown to reduce the expression of GLUT4 (Powelka et al., 2006) and its trafficking at the cell membrane (Ho et al., 2009).

RIP140 plays crucial roles in solid tumors (Lapierre et al., 2015). In colorectal cancers, RIP140 regulates the APC/β-catenin pathway and inhibits the proliferation of intestinal cells. Moreover, RIP140 acts as a tumor suppressor, high expression of RIP140 correlating with good prognosis of colorectal cancer patients (Lapierre et al., 2014). In breast cancer, we, and other groups, have reported that RIP140 promotes (Aziz et al., 2015; Rosell et al., 2014; Yu et al.,

2018) or impairs mammary tumor cell proliferation (Docquier et al., 2010; Jalaguier et al., 2017). Whether RIP140 is involved in the glucose metabolism of cancer cells and, if so, whether this directly affects tumor proliferation is still unknown.

Here we simultaneously characterized the effects of RIP140 on proliferation and glycolysis of cancer cells. We knocked-down RIP140 expression in human breast cancer cells and used immortalized and transformed mouse embryonic fibroblasts from RIP140 knockout (RIPKO) mice. We evaluated the survival of RIP140-deficient cells after disrupting glycolysis and characterized the mechanisms by which RIP140 regulates glycolysis in breast cancer cells to influence their growth. In line with these data, RIP140 expression correlates with good prognosis in breast cancer patients defined by a signature of the newly identified target gene and transcription partners.

Results

RIP140-deficiency promotes cell proliferation and tumor growth.

As mentioned above, opposite effects of RIP140 on human breast cancer cell proliferation have been described. Aiming to clarify this situation, we evaluated the impact of RIP140 silencing after small interfering RNA (siRNA) knockdown with two separate siRNAs on the proliferation of MCF7 and MDA-MB-436 breast cancer cell lines.

As shown by xCELLigence real-time cell analysis and MTT assays (Fig. 1a, b and Supplementary Fig. 1a-d), RIP140 silencing consistently increased cell proliferation confirming our previous results (Docquier et al., 2010; Jalaguier et al., 2017). To further validate the antiproliferative activity of RIP140 on human cancer cells, we performed the same type of experiments in prostate (DU145) and colon (RKO) human cancer cell lines. As shown in Supplementary Fig. 1e, knocking-down RIP140 expression in these cancer cells robustly increased proliferation in our experimental conditions.

We also studied the proliferation of mouse embryonic fibroblasts (MEFs) knocked-out for the *Rip140* gene (RIPKO, Supplementary Fig. 1f). 3T3-immortalized RIPKO MEFs proliferated more than 3T3-immortalized MEFs expressing *Rip140* (WT), as shown by xCELLigence and MTT assays (Fig. 1c and Supplementary Fig. 1g). Immortalized RIPKO cells

expressed more the proliferation markers, Cyclin A and Phosphorylated Serine10-Histone 3, and were richer in ATP (Fig. 1d and Supplementary Fig. 1h). In SV40-HRas/V12-transformed MEFs, RIP140-deficiency increased the cell proliferation and the number of colonies as shown, respectively, by MTT and soft agar assays (Supplementary Fig. 1i, j). To confirm the role of RIP140 in the observed effects, we rescued RIP140 expression by generating stable MEFs expressing either GFP or human RIP140 (Supplementary Fig. 1k). Rescuing RIP140 expression inhibited cell proliferation (Fig. 1e and Supplementary Fig. 1l), and reduced colony number (Fig. 1f and Supplementary Fig. 1m).

As the above data built a strong case for a growth inhibitory role of RIP140, we wondered whether RIP140 could also impact tumor growth. We therefore xenografted transformed RIPKO MEFs into nude mice and found that, indeed, these tumors had enhanced growth (Fig. 1g and Supplementary Fig. 1n, o). Altogether, our findings strongly push toward an anti-proliferative effect of RIP140 on cancer cell proliferation.

Inhibiting glycolysis reduces the growth advantage of RIP140-deficient cells.

As glucose homeostasis is a key parameter in the control of tumor cell proliferation, we sought to determine the importance of glucose for RIP140-deficient cell growth. We first

performed glucose starvation experiments and monitored cell proliferation. Lowering glucose concentrations affected RIPKO cell proliferation more than WT cells (Fig. 2a and Supplementary Fig. 2a). As shown in Supplementary Fig. 2b, the growth advantage of RIPKO cells observed in glucose-rich medium was abolished in the absence of glucose.

Upon glucose starvation, previous work reported that transformed MEFs displayed morphological features of cell death, such as loss of plasma membrane integrity and cell fragmentation (Chiaradonna et al., 2006). Transformed RIPKO MEFs displayed more features of dead cells than WT cells (Fig. 2b). Furthermore, we found that transformed RIPKO MEFs were more sensitive to glucose limitation than transformed WT MEFs (Supplementary Fig. 2c). These data suggested that RIP140-deficiency triggered glucose starvation-induced cell death.

Next, we analyzed cell viability after glycolysis blockade with the hexokinase inhibitor 2-deoxyglucose (2DG). As for glucose starvation, 2DG treatment abolished the RIPKO cell growth advantage (Fig. 2c and Supplementary 2d). Moreover, treatment with the GAPDH inhibitor 3-Bromopyruvate (BrP) induced the same response (Supplementary Fig. 2e). Cell proliferation and ATP level were more reduced in RIPKO MEFs under 2DG treatment (Fig 2d, e and Supplementary Fig. 2f). Moreover, RIPKO cells formed no colonies in the presence of the drug (Fig. 2f and Supplementary Fig. 2g). In preclinical models, to treat engrafted nude

mice with 2DG led to a greater reduction in volume of RIPKO than WT tumors (Fig 2g). Finally, both glycolysis inhibitors reduced the viability of MDA-MB-436 cells more efficiently when RIP140 was silenced by siRNA (Fig. 2h and Supplementary Fig. 2h).

Altogether, these results demonstrate that the growth advantage of RIP140-deficient cells is abolished when glycolysis is impaired. Therefore, RIP140-deficient cells rely on glycolysis to grow, suggesting that RIP140 inhibits cell proliferation by blocking glycolysis.

RIP140-deficiency enhances glycolysis in cancer cells.

Because these results suggested that RIP140 inhibits glycolysis in tumor cells, we characterized the glycolytic properties of RIP140-deficient cells. To do so, we performed Seahorse flux analysis that allow the measurement of the glucose-induced extracellular acidification rate, reflecting glycolysis. When basal extracellular acidification rate was set up as reference for each cell line, this acidification rate was higher in RIPKO cells (Fig. 3a). Further, the glycolytic parameters provided by the Agilent Wave software, including glycolysis, glycolytic capacity and glycolysis reserve, were higher in RIPKO MEFs (Fig. 3b). The high glycolysis content of RIPKO cells was confirmed in transformed MEFs (Supplementary Fig. 3a). Furthermore, glucose consumption and lactate production were higher in RIPKO cells,

confirming the Seahorse analysis (Fig. 3c, d). We also demonstrated that glucose uptake was higher in immortalized and transformed RIPKO MEFs (Fig. 3e). Then, rescuing RIP140 expression reduced extracellular acidification, confirming the inhibitory effect of RIP140 on glycolysis (Fig. 3f). Finally, silencing RIP140 by siRNA in MCF7 and MDA-MB-436 human breast cancer cells increased glycolysis (Fig. 3g and Supplementary 3b). Similar results were obtained in prostate and colon cancer cell lines (Supplementary Fig. 3c).

Thus, taken together, these results demonstrate that the loss of RIP140 increased glycolysis in cancer cells.

GLUT3 is essential for the growth advantage of RIP140-deficient cells.

To investigate how RIP140 regulates glycolysis in cancer cells, we monitored by RT-qPCR the expression of 23 different metabolic genes involved in glycolysis, in WT and RIPKO immortalized MEFs. The mRNA levels of *Glut3*, *Glut4* and *Ldhb* (Lactate Dehydrogenase B) were increased more than 2-fold in RIPKO MEFs (Supplementary Fig. 4a). The increase of *Glut3* mRNA expression level was the most important and was recapitulated in transformed MEFs (Supplementary Fig. 4b). Furthermore, this gene was also significantly increased by RIP140 silencing in the breast cancer cell lines MDA-MB-436 and MCF7 (Fig. 4a and

Supplementary Fig. 4c), whereas the *LDHB* and *GLUT4* levels did not change significantly (data not shown). Furthermore, rescuing RIP140 expression in RIPKO MEFs down-regulated *Glut*3 expression (Fig. 4b).

To investigate the mechanism by which RIP140 inhibits *GLUT3* expression, we first showed by luciferase reporter assays using the *GLUT3* promoter that RIP140 knock-down increased the luciferase activity of this reporter in MDA-MB-436 and MEF cells (Fig. 4c, d) and that RIP140 overexpression decreased it in MEF cells (Fig. 4d).

By chromatin immunoprecipitation (ChIP) assay in MDA-MB-436 cells , we observed the recruitment of RIP140 to the *GLUT3* promoter, indicating that the regulation by RIP140 occurred directly at the transcriptional level (Fig. 4e). Altogether, these data identify the *GLUT3* gene as a new transcriptional target of the transrepressive activity exerted by RIP140.

To evaluate to which extent RIP140-deficient cells needed GLUT3 to grow, we first validated the induction of GLUT3 at the protein level in MEFs (Supplementary Fig. 4d) and then knocked it down with small hairpin RNA (shRNA) in MEFs (Supplementary Fig. 4e). Knocking down GLUT3 abrogated the growth advantage induced by RIP140-deficiency as shown by either colony formation (Fig. 4f) or MTT (Fig. 4g) assays in MEFs. In MDA-MB-436 breast cancer cells, *GLUT3* silencing by siRNA abolished also the growth advantage

provoked by RIP140 silencing (Fig. 4h and Supplementary Fig. 4f). Altogether, these data show that the increase of cell proliferation upon RIP140-deficiency requires *GLUT3* induction.

RIP140 and p53 inhibit the expression of GLUT3 induced by HIF-2α.

One direct DNA binding factor that could likely mediate RIP140 activity is p53, as it is a well-known inhibitor of the Warburg effect (Gomes et al., 2018). Thus, we investigated whether p53 mediated any of the transcriptional activities of RIP140 on *GLUT3* expression. Using a luciferase reporter assay, we showed that increasing doses of p53 inhibited the luciferase activity driven by the *GLUT3* promoter (Fig. 5a), and that RIP140 reinforced this inhibition (Fig 5b). Of interest, RIP140 deficiency resulted in decreased p53 expression at the protein and mRNA levels. (Fig. 5c and Supplementary Fig. 5a). Therefore, RIP140-deficient cells exhibit many of the characteristics of cells under hypoxia such as cell proliferation, increased glycolysis and inactivation of p53 (Amelio and Melino, 2015).

To investigate the role of hypoxia in *Glut3* overexpression upon RIP140-deficiency, we first up-regulated the HIFs with a luciferase gene reporter driven by the *GLUT3* promoter. We found that the overexpression of HIF-2α, but not HIF-1α, increased the activity of the *GLUT3* promoter (Fig. 5d). Indeed, HIF-1α regulatory regions on *GLUT3* gene are not located within the promoter region (Mimura et al., 2012). We also found that HIF-2α, and not HIF-1α, was overexpressed in RIP140-deficient cells (Fig. 5e and Supplementary Fig. 5a). Interestingly, HIF-2α silencing reduced the expression of *Glut3*, only in RIP140 KO MEFs, suggesting that HIF-2α is responsible, at least in part, for *Glut3* overexpression upon RIP140 deficiency (Fig. 5f and Supplementary Fig. 5b).

To evaluate whether RIP140 could target HIFs activity, we first measured the effect of RIP140 on the transcriptional activity of HIFs using a luciferase reporter assay. We found that the transcriptional activity of a reporter gene containing hypoxia-response elements was higher in RIPKO than in WT MEFs and that increasing doses of RIP140 repressed the basic activity of this reporter gene (Fig. 5g). p53 is known to inhibit the transcriptional activity of HIFs (Blagosklonny et al., 1998). We then wondered whether RIP140 and p53 could cooperate to inhibit HIF transcriptional activity. We first looked at the effect of RIP140 or p53 individually on the transcriptional activity of the reporter gene containing hypoxia-response elements when transactivated by HIF-1α or HIF-2α. RIP140 or p53 were both capable of inhibiting HIF-α transcriptional activity separately (Fig. 5h and Supplementary Fig. 5c). Of interest, the repressive activity was stronger when RIP140 and p53 were expressed together, suggesting that RIP140 and p53 cooperate to inhibit HIF-α transcriptional activity (Fig. 5i and Supplementary Fig. 5d). The same synergistic repressive effect was observed on the *GLUT3* promoter when transactivated by HIF-2α (Fig. 5j).

Performing a proximity ligation assay demonstrated that HIF-2α, p53 and RIP140 interacted with each other (Fig. 5k). Altogether, these data suggested that the molecular mechanisms by which RIP140 inhibits *GLUT3* transcription relies on the repression of HIF transactivation through the formation of a ternary complex with p53.

The prognostic value of RIP140 is correlated with the levels of GLUT3 expression

Our experimental data demonstrated that RIP140 inhibits efficiently GLUT3 expression in synergy with p53, by antagonizing HIF-2α function, leading to a decrease in cancer cell

proliferation. We therefore hypothesized that, in breast cancers, low GLUT3 levels could be a marker of such anti-tumor activity of RIP140 and therefore, that RIP140 might be associated with an increased overall survival for patients with tumor expressing a reduced level of GLUT3, as a surrogate of RIP140 anti-tumor activity.

Using Cox proportional hazard regression (Nagy et al., 2021), we analyzed RNAseq data obtained from 1068 breast tumor samples from the TCGA dataset as described previously (Györffy et al., 2010) (Fig. 6). We first checked the prognostic values of the expression of each gene by analyzing patient overall survival (OS) at 60 months. High RIP140 expression was correlated with good prognosis whereas high GLUT3 was associated with bad prognosis (Fig. 6a).

Then we used the median as a cutoff value for classification of patients into two groups of tumors with low and high GLUT3 expression, respectively. Using Kaplan-Meier plots, we investigated whether RIP140 expression correlated with OS at 60 months within both groups using the same cutoff values. Interestingly, and as expected, RIP140 expression was significantly associated with increased OS in low GLUT3 expression group but not in high GLUT3 expression group (Fig. 6b).

We pursued our hypothesis by analyzing the prognostic value of RIP140 based on p53 (TP53), HIF-2α (EPAS1) and HIF-1α (HIF1A) expression levels. Patients were stratified again into low and high expression groups by using, as cutoff values, the median of either TP53, HIF-2α, or HIF-1α expression (Fig. 6c and Supplementary Fig. 6a). Strikingly, RIP140 expression was significantly associated with good prognosis in high p53 and low HIF-2α or HIF-1α expression groups, confirming the mechanism of RIP140 anti-tumor activity provided by our experimental data (Fig. 6c). Moreover, the prognostic value of RIP140 was significantly associated with good prognosis in low GLUT3 expression group but not in high GLUT3 expression group in colon and stomach cancers, suggesting that a reduced level of GLUT3 could reflect RIP140 anti-tumor activity in other types of cancer (Supplementary Fig. 6b).

Discussion

Glycolysis is essential for supporting the rapid proliferation of tumor cells. Our data reveal that the transcription coregulator RIP140 inhibits the glycolysis-dependent proliferation of breast cancer cells by impeding glycolysis through the blockade of *GLUT3* expression *via* a mechanism involving a p53-mediated inhibition of HIF activation.

Our results first demonstrate that the **glucose deprivation or glycolysis blockade abolished the gain in tumor cell proliferation caused by the decrease or loss of RIP140 expression**, showing the glucose dependency of RIP140-deficient cells. Furthermore, our data demonstrate that **down-regulating *Glut3* expression provoked the same inhibition of RIP140-deficient cell proliferation**. Of note, transformed RIPKO cells were more sensitive to glucose starvation than immortalized MEFs, suggesting that RIP140-deficiency might influence the transformation process by regulating glycolysis (Fig. 2b and Supplementary Fig. 2a). Interestingly, RIP140 does not regulate the metabolism of glutamine although this amino acid is also important for the proliferation of cancer cells (Jin et al., 2016). Indeed, the proliferation of WT and RIP140 KO cells was equally impacted by glutamine deprivation (data not shown), suggesting that RIP140 specifically affects glycolysis.

Our tailored experiments describe the **mechanism by which RIP140 inhibits *GLUT3* expression, which relies on the cooperation of RIP140 and p53** to inhibit the expression of *GLUT3* induced by HIF-2α (Fig. 5g). Indeed, proximity ligation assays allowed us to visualize the three partners in close proximity two-by-two, suggesting that they are involved in a ternary complex (Fig. 5h). Our data reveal for the first time that RIP140 interacts with p53 and HIF. Whether there is a ternary complex or if the interactions follow a temporal order will need to

be defined in future studies. It is tempting to speculate that RIP140 could act as an integrator protein such as CBP/p300 as p53 and HIF antagonism relies on competition for p300 (Schmid et al., 2004). RIP140 could enter into the competition with CBP as it does for nuclear receptors (Chen et al., 2004). The interplay between p53 and HIFs remains a complex question and it is still debated whether their reciprocal influence has any direct consequences for metabolism in cancer. Our results add RIP140 as a new major player in this interplay, and provide an additional bond between cell metabolism and cancer progression.

The overexpression of *GLUT3* has been described in many types of cancer with poor outcomes (Benito et al., 2017). In breast cancer patients, we found that **RIP140 is associated with an increased overall survival of patients with tumor expressing a reduced level of GLUT3**, as a surrogate of RIP140 anti-tumor activity (Fig. 6). Cellular metabolism in cancer is currently being targeted in clinical trials with some success (Sborov et al., 2015). Our results suggest that these genes could be used as a signature to identify patients that could benefit of therapies targeting glycolysis and/or based on HIF inhibitors.

Altogether, our results enable us to propose a new model explaining the transcriptional control of glycolysis-dependent cancer cell proliferation by a nuclear interplay between three actors that might be clinically relevant for breast cancer patients (Figure 7).

Acknowledgements

We thank Dr. Yuan, Dr. Karadimitris and Prof. Schymkowitz for the kind gift of plasmids, and Drs. Lapierre and Palassin for the generation of immortalized MEF #1 and stable MEF#1 overexpressing hRIP140, respectively. Thanks also to Dr. Stallcup for proofreading the manuscript. We gratefully acknowledge the financial support of ARC Foundation (R15083FF), Ligue Contre le Cancer (LNCC R13008FF, LNCC R15016FF), and Fondation pour la Recherche Médicale (N° DEQ20170336713).

Author contributions

V.J., D.G., S.F., L.K.L., S.B., S.J. and C.T. performed the experiments. S.F. and L.K.L contributed to the *in vivo* experiments. S.F. generated MEF #2. V.J. and S.J. performed breast cancer cell proliferation experiments. V.J. performed ChIP experiments, glycolysis inhibition and siRNA experiments in cancer cells, and glucose starvation experiments. D.G performed

immunoblots, ATP measurement, 2DG treatment experiments, cell proliferation assays in MEF#1. S.B. performed luciferase reporter assays. C.T. generated MEF #3 and #4, performed Seahorse, glucose uptake, xCELLigence, soft agar, PLA, shRNA experiments, luciferase reporter assays and immunoblots. V.J, V.C. and C.T. designed the studies and interpreted the data. C.T. wrote the manuscript. V.C. reviewed and approved the manuscript. All authors discussed and revised the manuscript. V.J. was supported by a fellowship from the French Ministry of Research.

Data Availability

Source data for all the figures are provided with the paper. All materials are available upon request to the corresponding authors.

Competing Interests statement

The authors declare no competing financial interests.

Materials and Methods

Plasmids and reagents.

RIP140-expressing vectors (pEFcmyc-RIP140 (Carascossa et al., 2006), pEGFP-RIP140 (Zilliacus et al., 2001)) and control vectors, pEGFP (Clontech), are described elsewhere. HA-HIF1alpha-pcDNA3 (Addgene plasmid # 18949) and HA-HIF2alpha-pcDNA3 (Addgene plasmid # 18950) plasmids were gifts from Dr Kaelin (Kondo et al., 2002). The GLUT3-Luc reporter gene was a gifts from Dr. Yuan (Liu et al., 2014).. 2-Deoxy-D-glucose (2DG, D6134)), 6-Aminonicotinamide (6AN; # A68203), 3-Bromopyruvate (BrP; #16490), MTT ((3- (4,5-dimethylthiazol-2-yl)-2,5-diphenyl tetrazolium bromide) (98%, CAS 298-93-1), Deferoxamine mesylate salt (D9533), Di(N-succinimidyl) glutarate (80424), crystal violet (C0775), anti-Mouse IgG-FITC antibody (F6257), monoclonal Anti-ß-Actin-Peroxidase antibody (A3854) were purchased from Sigma-Aldrich (Merck, Darmstadt, Germany). Puromycin (ant-pr-1) was purchased from Invivogen (France). The ATP Determination Kit (10700345) was from Fisher Scientific (France). Deoxy-D-glucose, 2-[1,2-3H (N)] (NET328A250UC) was from Perkin Elmer (France). GLUT3 shRNA (m) (sc-41219-V) were purchased from Santa Cruz Biotechnology (Dallas, USA). Rabbit polyclonal to RIP140 (ab42126) was from Abcam

(Cambridge, UK). BrdU Hu-purified-clone B44 (#347580) was from Becton Dickinson (France).

Cell culture. Immortalized and transformed mouse embryonic fibroblasts (MEFs) were cultured in F12/Dulbecco's modified Eagle's medium supplemented with 10% fetal calf serum, 1% Penicillin/Streptomycin, 1mM Sodium Pyruvate and 10mM HEPES. Primary MEFs were prepared from 13.5 day wild-type (WT) or RIPKO mouse embryos (White et al., 2000) and genotyped by PCR. All experiments on mice were performed in accordance with French guidelines (agreement n° 201603101538202). Immortalized MEFs were obtained by sequential passage, according to the 3T3 protocol (Todaro and Green, 1963), or by infection with retrovirus expressing SV40. After immortalization, MEFs were transformed with retrovirus expressing H-RasV12. Virus production, infection and transfection were performed as previously described (Rodier et al., 2015). Stably infected cells were selected with Puromycin (2.5µg/ml) after SV40 virus infection and Hygromycin (65µg/ml) after H-RasV12 virus infection. Four independently derived RIP140 WT and RIPKO MEF cell lines were established. MEF#1 were immortalized by the 3T3 protocol. MEF#2, #3 and #4 were transformed by the infection of SV40/H-RasV12 expressing retrovirus. Immortalized MEF#1 were transduced with lentiviral particles expressing shRNA against murine GLUT3 (sc-41219-V) according to

the manufacturer's protocol (Santa Cruz Biotechnology,). MEFs transfected with pEGFP or pEGFP-hRIP140 were cultured in the presence of 3.2µg/ml Puromycin, as the selection agent to establish stable cell lines. MCF7, PC3 and DU145 were cultured in F12/Dulbecco's modified Eagle's medium supplemented with 10% fetal calf serum, 1% Penicillin/Streptomycin. MDA-M-B436 and RKO were cultured in Dulbecco's Modified Eagle Medium (DMEM) + GlutaMax (Thermo Fisher Scientific; Waltham, MA), supplemented with 10% FBS and 1% Penicillin/Streptomycin.

Real-time qPCR. Real-time qPCR was conducted as previously described (Jalaguier et al., 2017). Briefly, total RNA was extracted from cells using the Quick RNA™ Miniprep kit (Zymo Research, Irvine, CA, USA) according to the manufacturer's instructions. cDNA was synthetized with 1 µg of RNA and the qScript cDNA master mix (Quanta Bio, Beverly, MA, USA). mRNA expression was determined with a quantitative real time PCR SYBR Green SensiFAST™ SYBR® No-ROX Kit (Bioline, London, UK) on a Light Cycler® 480 Instrument II (Roche Life Sciences). Relative expression levels for the mRNAs of interest were normalized to 28S or RS9 housekeeping genes. See Supplemental Table 1 for the list of primer sequences.

Protein detection.

Protein expression was quantified by western blot analysis using the following antibodies: anti-cyclin A (1:500 sc-751; Santa Cruz Biotechnology, Dallas, TX, USA), anti-Histone H3 (phospho Serine10) (1:2,000 ab14955; Abcam Cambridge, UK), anti-GLUT3 (1:10000 ab191071; Abcam), anti-p53 (1:1000 1C12; Cell Signaling Technology, Leiden, The Netherlands), anti-HIF-1α (1:1000 NB100-105; Novus Biologicals, LLC (Centennial, USA)), anti-HIF-2α/EPAS1 (1:1000 NB100-122; Novus Biologicals, LLC (Centennial, USA)), and anti-Actin-HRP (1:10000 A3854, Merck, Darmstadt, Germany).

Immunofluorescence, proximity ligation assays (PLA) and GST-pull down were performed as described (Jalaguier et al., 2017).

Luciferase assay. For gene reporter assays, cells were plated in 96-well plates and transfected with JetPEI (Polyplus, Illkirch-Graffenstaden, France) according to the manufacturer's protocol. Data were expressed as relative firefly luciferase activity normalized to renilla activity. For all experiments, data were collected from at least three biological replicates.

Chromatin immunoprecipitation. Approximately one hundred and twenty million cells were harvested per experiment. Briefly, protein–DNA complexes were first cross-linked, using 2mM Di (N-succinimidyl) Glutarate (DSG), for 50 min on a rotor, then the procedure was performed using High-Sentivity kit (Active Motif, Shanghai) and according to manufacturer's protocol.

Chromatin was sonicated for thirty seconds on ice followed by thirty seconds off, for a total of thirty minutes. Immunoprecipitations were performed with 30µg of protein-DNA complexes and 4µg of RIP140 antibody (Ab42126; Abcam). The purified DNAs were amplified with SYBR Green SensiFAST™ SYBR® No-ROX Kit (Bioline, London, UK) by real-time qPCR.

Cell growth analysis

MTT assay. Cell proliferation assays were performed using MTT as previously described (Jalaguier et al., 2017). Data were normalized to the absorbance value at day 1. Experiments were performed three times with at least sextuplets. For glucose starvation experiments, cells grew for 24 hours in complete media. Then cells were washed twice with PBS and starvation medium (DMEM5030 supplemented with 10% dialyzed FBS, 2mM Glutamine, 1% Penicillin/Streptomycin, HEPES 10mM, 1mM Sodium Pyruvate, 3.7g/l Sodium Bicarbonate) was added to the cells supplemented, or not, with indicated glucose concentrations.

xCELLigence analysis. The Real-time Cell Analyzer DP instrument (Agilent, Santa Clara, USA) was placed in a humidified incubator maintained at 37ºC with 5% CO_2. Cells were plated at 1500 cells/well into 16-well E-Plates. The impedance value of each well was automatically monitored every hour for up to the indicated times by the xCELLigence system. Cell

proliferation is represented by an index that reflects changes in electrical impedance matching to cellular coverage of the electrode sensors.

Soft agar colony assay. Soft agar experiments were performed as described previously (Rodier et al., 2015). Briefly, transformed MEFs (8.10^4 cells) were mixed with culture medium containing 0.4% agar and seeded into 6-well plates coated with 1% agar in F12/DMEM containing 10% FBS in at least triplicate. Medium was changed twice a week. After 20 days, colonies were stained with 0.5% crystal violet solution, photographed and counted with ImageJ software.

Mouse xenograft assays. Transformed MEF ($5.\ 10^5$ cells) were resuspended in 100 µl of RPMI medium (Thermo Fisher Scientific; Waltham, MA) and injected subcutaneously into the dorsal area of 4-6 week-old immuno-deficient athymic female mice (Charles River, Écully, France). After 10-14 days, tumor volumes were measured every 3-4 days with a caliper. Before reaching tumor volume limit point, fibrosarcomas were excised, photographed and weighed.

Metabolic measurements

Glucose uptake. One day after cell seeding at 50,000 cells/well into 24-w plates, cells were washed once with PBS and medium was replaced with low-glucose medium (DMEM5030

supplemented with 10% dialyzed FBS (Thermo Fisher Scientific, Waltham, MA), 2mM Glutamine, 1% Penicilline/Streptomycin, HEPES 10mM, 1mM Sodium Pyruvate, 3.7g/l Sodium Bicarbonate, 0.25mM Glucose). Then 1µCi/ml of Deoxy-D-glucose, 2-[1,2-3H(N)] (Perkin Elmer, Waltham, MA) was added for 30 minutes at room temperature. Cells were washed once with PBS and then lysed with 200µl of 1%SDS; 10mM Tris pH 7.5. 100µl was used to count radioactivity with a Perkin Elmer liquid scintillation analyzer Tri-Carb 2900TR and 5µl was used to quantify proteins for normalization.

Cellular ATP measurement. ATP content was determined using the ATP determination kit according to the manufacturer's instructions (Molecular Probes, Thermo Fisher Scientific,Waltham, MA). Cells were washed with iced-cold 1x PBS and extracted in an ATP-releasing buffer containing 100 mM potassium phosphate buffer at pH 7.8, 2 mM EDTA, 1 mM dithiothreitol, and 1% Triton X-100. Then, 5 µl of lysate was used for protein determination by the DC Protein Assay (Bio-Rad Laboratories, Hercules, CA). ATP levels were expressed in nM ATP per 10 µg protein units and then normalized with respect to the level in control samples.

Seahorse experiments. Extracellular acidification rate (measured in mpH/min) was monitored using an XFe24 extracellular flux analyzer from Seahorse Bioscience (Agilent, Santa Clara, CA) following the manufacturer's protocol. Experiments were carried out on confluent

monolayers. Briefly, cells were seeded 24 hours before experiments at a density of 35,000 cells/well (24-well). Before starting measurements, cells were washed once with PBS and medium was replaced with Seahorse XF Base Medium supplemented with 2mM glutamine without glucose at pH 7.4) and were placed into a 37 °C non-CO2 incubator for 1 hour prior to the assay. Glucose, oligomycin, and 2-DG were diluted into XF24 media and loaded into the accompanying cartridge to achieve final concentrations of 10 mM, 1 μm, and 100 mM, respectively. Injections of the drugs into the medium occurred at the time points specified. Each cycle consisted of 3 min mixing, 3 min waiting and 3 min measuring. Data were transformed with Agilent Seahorse Wave software to export glycolysis parameters. Values were expressed after normalization to the protein content of each well and to the values just before glucose addition. Acidification rates were presented as the mean ± SD of 4 to 6 replicate wells.

Glucose and Lactate assays. Cells were seeded in culture dishes and cultured for 8 h. The culture medium was then changed and cells were incubated for an additional 16 h. Subsequently, the culture medium was collected for determination of glucose concentration and lactate levels using a Glucose assay kit (Amplite ™ Glucose Quantitation Assay kit, AAT Bioquest, Sunnyvale, CA) and a Lactate assay kit (MAK064, Merck, Darmstadt, Germany) according to the manufacturer's instructions. Glucose consumption was calculated as the

difference in glucose concentration between fresh medium and cell supernatant. Lactate production was determined as the difference in lactate concentration between cell supernatant and fresh medium. Data were normalized to final cell counts and time.

Survival analysis. RNA sequencing (RNA-seq) data were utilized from the Cancer Genome Atlas (TCGA) using the KM-plot Private Edition (http://kmplot.com) (Györffy et al., 2010). Using Cox proportional hazards regression, RNAseq data obtained from breast cancer samples were analyzed as previously described (Nagy et al., 2021). The Kaplan-Meier method was used to estimate overall survival calculated from diagnosis to death. Patients lost to follow-up were censored at the time of last contact.

Statistical analysis. Data are expressed as mean ± SD. Unless stated otherwise, statistical analysis was performed by a Mann-Whitney test using StatEL. The p values less than 0.05 were considered to be statistically significant (***$p < 0.001$, **$p<0.01$, *$p < 0.05$).

Table1. Murine primer sequences

Name	Sequence
ALD1-FOR	TTCGCCTACCCACCGGCGTA
ALD1-REV	GGTGGCAGTGCTTTCCTGGCA
ALDOC-FOR	ACCATATTGGGCTTGAGCAG

ALDOC-REV	CCTCAAACGTTGCCAGTATGT
ENO1-FOR	AAAGATCTCTCTGGCGTGGA
ENO1-REV	CTTAACGCTCTCCTCGGTGT
ENO3-FOR	GGACTCCAGGGGCAACCCCA
ENO3-REV	TGCTCGGAATCGACCCTTGGC
GAPDH-FOR	GTGCAGTGCCAGCCTCGTCC
GAPDH-REV	CAGGCGCCCAATACGGCCAA
GLUT1-FOR	GAGTGTGGTGGATGGGATG
GLUT1-REV	AACACTGGTGTCATCAACGC
GLUT2-FOR	GGCTAATTTCAGGACTGGTT
GLUT2-REV	AACCAGTCCTGAAATTAGCC
GLUT3-FOR	ATCGTGGCATAGATCGGTTC
GLUT3-REV	TCTCAGCAGCTCTCTGGGAT
GLUT4-FOR	CAGTGTTCCAGTCACTCGCT
GLUT4-REV	TTTTAAAACAAGATGCCGTCG
GPI1-FOR	AAAGTCCAATGGCTGACCAC
GPI1-REV	CACGGCCAAAGTGAAAGAGT
HIF1-FOR	AAACTTCAGACTCTTTGCTTCG
HIF1-REV	CGGCGAGAACGAGAAGAA
HIF2-FOR	ATC ACG GGA TTT CTC CTT CC
HIF2-REV	GGT TAA GGA ACC CAG GTG CT
HK2-FOR	GGAACCGCCTAGAAATCTCC
HK2-REV	GGAGCTCAACCAAAACCAAG
LDHA-FOR	GCAACATTCACACCACTCCA
LDHA-REV	TCCGTTACCTGATGGGAGAG
LDHB-FOR	GCTGCAGGTCCATCATCTCT
LDHB-REV	GTTGGACAAGTGGGTATGGC
PDK2-FOR	TTCCATGATGTCCAGCAGAC
PDK2-REV	GATCAACCTGCTTCCTGACC
PDK1-FOR	TTACTCAGTGGAACACCGCC
PDK1-REV	GTTTATCCCCCGATTCAGGT

PDK3-FOR	GTTAGCCAGTCGCACAGGA
PDK3-REV	CGTCGCCACTGTCTATCAAA
PDK4-FOR	TGACAGGGCTTTCTGGTCTT
PDK4-REV	AGTGAACACTCCTTCGGTGC
PFK2-FOR	AATGAGTGTTGGGGAGTTGG
PFK2-REV	CAGAAGACTGCAACAGCAGC
PFK3-FOR	CCACCATCACAATCACGGT
PFK3-REV	CAGAGCCGGGTACAGAAGAT
PG1-FOR	GTTCTTCAATGGCACCGACT
PG1-REV	AGTGGGACTGAGCCCAAAAT
PGK1-FOR	CAGCCTTGATCCTTTGGTTG
PGK1-REV	CTGACTTTGGACAAGCTGGA
PKM2-FOR	GCCGCCTGGACATTGACTC
PKM2-REV	CCA TGAGAGAAATTCAGCCGAG
p53-FOR	GAAGTCCTTTGCCCTGAAC
p53-REV	CTAGCAGTTTGGGCTTTCC
TPI1-FOR	AAAGTCGATGTAAGCGGTGG
TPI1-REV	GAAGTGCCTGGGAGAACTCA

Table 2. ChIP primer sequences

Name	Séquence	Ref
NegCHIP-FOR	ATGGTTGCCACTGGGGATCT	(Liu et al., 2014)
NegCHIP-REV	TGCCAAAGCCTAGGGGAAGA.	(Liu et al., 2014)

GLUT3CHIP-FOR	CCCCTGAAGCAATCTTGTGATC	(Liu et al., 2014)
GLUT3CHIP-REV	AAAAA CCCAGGGTGGAGAGAG	(Liu et al., 2014)

Table 3. siRNA sequences.

Name	sequence	Ref
siControl	(UAAUGUAUUGGAACGCAUA)TT	
siRIP140-1=#2	(AUACGAAUCUUCCUGAUGU)TT	
siRIP140-4=#1	(GAAGCGUGCUAACGAUAAA)TT	
siHIF1mouse	(AAAGGACAAGUCACCACAGGA)TT	(Mi et al., 2008)
siHIF2mouse	(AAGUCACCAGAACUUGUGCAC)TT	(Mi et al., 2008)

References

Amelio, I., and Melino, G. (2015). The p53 family and the hypoxia-inducible factors (HIFs): determinants of cancer progression. Trends Biochem. Sci. *40*, 425–434.

Augereau, P., Badia, E., Balaguer, P., Carascossa, S., Castet, A., Jalaguier, S., and Cavaillès, V. (2006). Negative regulation of hormone signaling by RIP140. J. Steroid Biochem. Mol. Biol. *102*, 51–59.

Aziz, M.H., Chen, X., Zhang, Q., DeFrain, C., Osland, J., Luo, Y., Shi, X., and Yuan, R. (2015). Suppressing NRIP1 inhibits growth of breast cancer cells in vitro and in vivo. Oncotarget *6*, 39714–39724.

Benito, A., Polat, I.H., Noé, V., Ciudad, C.J., Marin, S., and Cascante, M. (2017). Glucose-6-phosphate dehydrogenase and transketolase modulate breast cancer cell metabolic reprogramming and correlate with poor patient outcome. Oncotarget *8*, 106693–106706.

Blagosklonny, M.V., An, W.G., Romanova, L.Y., Trepel, J., Fojo, T., and Neckers, L. (1998). p53 inhibits hypoxia-inducible factor-stimulated transcription. J. Biol. Chem. *273*, 11995–11998.

Carascossa, S., Gobinet, J., Georget, V., Lucas, A., Badia, E., Castet, A., White, R., Nicolas, J.-C., Cavaillès, V., and Jalaguier, S. (2006). Receptor-interacting protein 140 is a repressor of the androgen receptor activity. Mol. Endocrinol. *20*, 1506–1518.

Castet, A., Herledan, A., Bonnet, S., Jalaguier, S., Vanacker, J.-M., and Cavaillès, V. (2006). Receptor-interacting protein 140 differentially regulates estrogen receptor-related receptor transactivation depending on target genes. Mol. Endocrinol. *20*, 1035–1047.

Cavaillès, V., and Lapierre, M. (2014). Regulation of intestinal homeostasis and tumorigenesis by the transcriptional coregulator RIP140. Mol Cell Oncol *1*, e960761.

Chen, Y., Hu, X., and Wei, L.-N. (2004). Molecular interaction of retinoic acid receptors with coregulators PCAF and RIP140. Mol. Cell. Endocrinol. *226*, 43–50.

Chiaradonna, F., Sacco, E., Manzoni, R., Giorgio, M., Vanoni, M., and Alberghina, L. (2006). Ras-dependent carbon metabolism and transformation in mouse fibroblasts. Oncogene *25*, 5391–5404.

Docquier, A., Harmand, P.-O., Fritsch, S., Chanrion, M., Darbon, J.-M., and Cavaillès, V. (2010). The transcriptional coregulator RIP140 represses E2F1 activity and discriminates breast cancer subtypes. Clin. Cancer Res. *16*, 2959–2970.

Fritah, A. (2009). Control of skeletal muscle metabolic properties by the nuclear receptor corepressor RIP140. Appl Physiol Nutr Metab *34*, 362–367.

Gomes, A.S., Ramos, H., Soares, J., and Saraiva, L. (2018). p53 and glucose metabolism: an orchestra to be directed in cancer therapy. Pharmacol. Res. *131*, 75–86.

Györffy, B., Lanczky, A., Eklund, A.C., Denkert, C., Budczies, J., Li, Q., and Szallasi, Z. (2010). An online survival analysis tool to rapidly assess the effect of 22,277 genes on breast cancer prognosis using microarray data of 1,809 patients. Breast Cancer Res Treat *123*, 725–731.

Ho, P.-C., and Wei, L.-N. (2012). Biological activities of receptor-interacting protein 140 in adipocytes and metabolic diseases. Curr Diabetes Rev *8*, 452–457.

Ho, P.-C., Lin, Y.-W., Tsui, Y.-C., Gupta, P., and Wei, L.-N. (2009). A negative regulatory pathway of GLUT4 trafficking in adipocyte: new function of RIP140 in the cytoplasm via AS160. Cell Metab. *10*, 516–523.

Hsu, P.P., and Sabatini, D.M. (2008). Cancer cell metabolism: Warburg and beyond. Cell *134*, 703–707.

Humpton, T., and Vousden, K.H. (2019). Taking up the reins of power: metabolic functions of p53. 610–614.

Jalaguier, S., Teyssier, C., Nait Achour, T., Lucas, A., Bonnet, S., Rodriguez, C., Elarouci, N., Lapierre, M., and Cavaillès, V. (2017). Complex regulation of LCoR signaling in breast cancer cells. Oncogene *36*, 4790–4801.

Jin, L., Alesi, G.N., and Kang, S. (2016). Glutaminolysis as a target for cancer therapy. Oncogene *35*, 3619–3625.

Kawauchi, K., Araki, K., Tobiume, K., and Tanaka, N. (2008). p53 regulates glucose metabolism through an IKK-NF-kappaB pathway and inhibits cell transformation. Nat. Cell Biol. *10*, 611–618.

Kondo, K., Klco, J., Nakamura, E., Lechpammer, M., and Kaelin, W.G. (2002). Inhibition of HIF is necessary for tumor suppression by the von Hippel-Lindau protein. Cancer Cell *1*, 237–246.

Kuang, R., Jahangiri, A., Mascharak, S., Nguyen, A., Chandra, A., Flanigan, P.M., Yagnik, G., Wagner, J.R., Lay, M.D., Carrera, D., et al. (2017). GLUT3 upregulation promotes metabolic reprogramming associated with antiangiogenic therapy resistance. JCI Insight *2*.

Lapierre, M., Bonnet, S., Bascoul-Mollevi, C., Ait-Arsa, I., Jalaguier, S., Del Rio, M., Plateroti, M., Roepman, P., Ychou, M., Pannequin, J., et al. (2014). RIP140 increases APC expression and controls intestinal homeostasis and tumorigenesis. J. Clin. Invest. *124*, 1899–1913.

Lapierre, M., Docquier, A., Castet-Nicolas, A., Gitenay, D., Jalaguier, S., Teyssier, C., and Cavaillès, V. (2015). The emerging role of the transcriptional coregulator RIP140 in solid tumors. Biochim. Biophys. Acta *1856*, 144–150.

Liu, X.-S., Haines, J.E., Mehanna, E.K., Genet, M.D., Ben-Sahra, I., Asara, J.M., Manning, B.D., and Yuan, Z.-M. (2014). ZBTB7A acts as a tumor suppressor through the transcriptional repression of glycolysis. Genes Dev. *28*, 1917–1928.

Majmundar, A.J., Wong, W.J., and Simon, M.C. (2010). Hypoxia-Inducible Factors and the Response to Hypoxic Stress. Molecular Cell *40*, 294–309.

Metallo, C.M., and Vander Heiden, M.G. (2013). Understanding Metabolic Regulation and Its Influence on Cell Physiology. Molecular Cell *49*, 388–398.

Mi, Z., Rapisarda, A., Taylor, L., Brooks, A., Creighton-Gutteridge, M., Melillo, G., and Varesio, L. (2008). Synergystic induction of HIF-1alpha transcriptional activity by hypoxia and lipopolysaccharide in macrophages. Cell Cycle *7*, 232–241.

Mimura, I., Nangaku, M., Kanki, Y., Tsutsumi, S., Inoue, T., Kohro, T., Yamamoto, S., Fujita, T., Shimamura, T., Suehiro, J., et al. (2012). Dynamic Change of Chromatin Conformation in Response to Hypoxia Enhances the Expression of GLUT3 (SLC2A3) by Cooperative Interaction of Hypoxia-Inducible Factor 1 and KDM3A. Molecular and Cellular Biology *32*, 3018–3032.

Nagy, Á., Munkácsy, G., and Győrffy, B. (2021). Pancancer survival analysis of cancer hallmark genes. Sci Rep *11*, 6047.

Nautiyal, J. (2017). Transcriptional coregulator RIP140: an essential regulator of physiology. J. Mol. Endocrinol. *58*, R147–R158.

Patra, K.C., and Hay, N. (2014). The pentose phosphate pathway and cancer. Trends Biochem. Sci. *39*, 347–354.

Powelka, A.M., Seth, A., Virbasius, J.V., Kiskinis, E., Nicoloro, S.M., Guilherme, A., Tang, X., Straubhaar, J., Cherniack, A.D., Parker, M.G., et al. (2006). Suppression of oxidative metabolism and mitochondrial biogenesis by the transcriptional corepressor RIP140 in mouse adipocytes. J. Clin. Invest. *116*, 125–136.

Razungles, J., Cavaillès, V., Jalaguier, S., and Teyssier, C. (2013). [The Warburg effect: from theory to therapeutic applications in cancer]. Med Sci (Paris) *29*, 1026–1033.

Rodier, G., Kirsh, O., Baraibar, M., Houlès, T., Lacroix, M., Delpech, H., Hatchi, E., Arnould, S., Severac, D., Dubois, E., et al. (2015). The transcription factor E4F1 coordinates CHK1-dependent checkpoint and mitochondrial functions. Cell Rep *11*, 220–233.

Rosell, M., Nevedomskaya, E., Stelloo, S., Nautiyal, J., Poliandri, A., Steel, J.H., Wessels, L.F.A., Carroll, J.S., Parker, M.G., and Zwart, W. (2014). Complex formation and function of estrogen receptor α in transcription requires RIP140. Cancer Res. *74*, 5469–5479.

Sborov, D.W., Haverkos, B.M., and Harris, P.J. (2015). Investigational cancer drugs targeting cell metabolism in clinical development. Expert Opin Investig Drugs *24*, 79–94.

Schmid, T., Zhou, J., Köhl, R., and Brüne, B. (2004). p300 relieves p53-evoked transcriptional repression of hypoxia-inducible factor-1 (HIF-1). Biochem. J. *380*, 289–295.

Schwartzenberg-Bar-Yoseph, F., Armoni, M., and Karnieli, E. (2004). The Tumor Suppressor p53 Down-Regulates Glucose Transporters GLUT1 and GLUT4 Gene Expression. Cancer Res *64*, 2627–2633.

Sermeus, A., and Michiels, C. (2011). Reciprocal influence of the p53 and the hypoxic pathways. Cell Death Dis *2*, e164.

Todaro, G.J., and Green, H. (1963). Quantitative studies of the growth of mouse embryo cells in culture and their development into established lines. J. Cell Biol. *17*, 299–313.

Vander Heiden, M.G., Cantley, L.C., and Thompson, C.B. (2009). Understanding the Warburg effect: the metabolic requirements of cell proliferation. Science *324*, 1029–1033.

White, R., Leonardsson, G., Rosewell, I., Ann Jacobs, M., Milligan, S., and Parker, M. (2000). The nuclear receptor co-repressor nrip1 (RIP140) is essential for female fertility. Nat. Med. *6*, 1368–1374.

Yu, X.-H., Xue, X., Zhu, X., and Li, X. (2018). Downregulation of RIP140 in triple-negative breast cancer inhibits the growth and proliferation of cancer cells. Oncol Lett *15*, 8784–8788.

Zilliacus, J., Holter, E., Wakui, H., Tazawa, H., Treuter, E., and Gustafsson, J.A. (2001). Regulation of glucocorticoid receptor activity by 14--3-3-dependent intracellular relocalization of the corepressor RIP140. Mol. Endocrinol. *15*, 501–511.

Zong, W.-X., Rabinowitz, J.D., and White, E. (2016). Mitochondria and Cancer. Molecular Cell *61*, 667–676.

Zschiedrich, I., Hardeland, U., Krones-Herzig, A., Berriel Diaz, M., Vegiopoulos, A., Müggenburg, J., Sombroek, D., Hofmann, T.G., Zawatzky, R., Yu, X., et al. (2008). Coactivator function of RIP140 for NFkappaB/RelA-dependent cytokine gene expression. Blood *112*, 264–276.

Figure Legends.

Fig. 1. RIP140-deficiciency enhances cell proliferation and tumorigenesis.

a, b, Cell proliferation of breast cancer cells MCF7 (**a**) and (MDA-MB-436) (**b**) monitored by xCELLigence after silencing RIP140 by siRNA (representative experiment, n=2 independent experiments).

c, Cell proliferation monitored by xCELLigence in RIP140 WT and KO-immortalized MEFs (MEF #1) (n=3 independent experiments).

d, Western blot showing expression of Cyclin A, Phospho Serine 10-Histone 3 and Actin in MEF #1. Unprocessed original scans of blots are shown in Supplementary Figure 7.

e, Cell proliferation monitored by xCELLigence of MEF #1 WT stably overexpressing a pEGFP plasmid (WT+GFP, RIPKO+GFP) or RIPKO stably overexpressing a pEGFP-hRIP140 plasmid (RIPKO+hRIP140) (n=2 independent experiments).

f, Number of colonies of H-RasV12-transformed MEF #1 stably overexpressing pEGFP or pEGFP-hRIP140 obtained in a colony formation soft agar assay (n=4 independent experiments).

g, SV40/H-RasV12-transformed MEF (MEF #2) WT and RIPKO cells were injected subcutaneously into the flanks of immuno-deficient mice (n=7) to assess their tumorigenic

potential (left panel). The weight of the tumors were assessed six weeks after grafting (n=6 mice; right panel).

Fig. 2. Inhibiting glycolysis reduces the growth advantage of RIP140-deficient cells.

Unless otherwise stated, MEF #1 were used.

a, Cells were grown in medium whithout glucose. Cell proliferation analyzed by MTT assay was expressed relative to that of cells grown in Glucose 4.5g/L at day ten (representative experiment, n=3 independent experiments).

b, Microscopic morphological analysis of representative transformed MEF #3.

c, Cell proliferation analyzed by xCELLigence assay upon 2-deoxyglucose treatment (2DG; 5mM) (n=3 independent experiments). The slope of the curves was extracted using xCELLigence RTCA Software (right panel).

d, Cell number as percent of control following eight days of 2DG treatment (5mM) (n=3 independent experiments).

e, Cellular ATP content in MEF #1 after 3 days of 2DG treatment (5mM) expressed as percent of control (n=3 independent experiments).

f, Number of colonies from soft agar assay of transformed MEF #3 after 3 weeks of 2DG treatment (5mM).

g, Tumor volume of transformed MEF #1 xenografted in nude mice (n=6) after eighteen days of 2DG (20mg/g) administrated intra-peritoneally every other day.

h, Cell viability assessed by crystal violet staining of MDA-MB-436 after RIP140 silencing by siRNA at day seven and represented as percent of control after 2DG (5mM) treatment (n=3 independent experiments).

Fig. 3. RIP140-deficiency enhances glycolysis in breast cancer cells.

Unless otherwise stated MEF #1 were used.

a, Percentage change in extracellular acidification rate (ECAR) was monitored in real-time with a Seahorse Bioscience Flux Analyzer. Cells were treated sequentially with glucose (10 mM), oligomycin (1µM) and 2-DG (100 mM). Values were normalized by protein quantity (representative experiment, n=5 independent experiments).

b, XF Glycolysis Stress Test Parameters represented as percent of basal WT ECAR from data obtained in Fig. 3a.

c, **d**, Glucose consumption (**c**) and lactate production (**d**) were measured by enzymatic determination assay 18h after changing medium. Values were normalized to cell number and time.

e, [^{3}H] 2-Deoxy-D-glucose uptake in MEF #1, #3 and #4, relative to the WT group and normalized by protein quantity (representative experiment, n=2 independent experiments).

f, Glycolysis measured in MEF #1 overexpressing or not hRIP140 and represented by ΔECAR calculated as the difference between basal ECAR and ECAR after-glucose injection and normalized by that in MEF WT (representative experiments, n=3 independent experiments).

g, Glycolysis measured in breast cancer cell lines MCF7 and MDA-MB-436 after RIP140 silencing by siRNA and represented as previously (representative experiments, n=3 independent experiments).

Fig. 4. GLUT3 is essential for the growth advantage induced by RIP140-deficiency.

a, mRNA levels of *RIP140* and *GLUT3* quantified by RT-qPCR in MDA-MB-436 after RIP140 silencing by siRNA (n=3 independent experiments).

b, mRNA levels of *Glut3* quantified by RT-qPCR in MEF #1 overexpressing hRIP140 (n=3 independent experiments).

c, Luciferase assay in MDA-MB-436 transiently transfected with TK-Renilla, GLUT3-Luc reporter plasmids and increasing doses of siRNA (siRIP140). Luciferase values were normalized to the renilla luciferase control. Data shown are from one representative experiment done in triplicates (Student-t-Test).

d, Luciferase assay in MEF #1 transiently transfected with TK-Renilla, GLUT3-Luc reporter plasmids and increasing doses of c-Myc-RIP140 vector. Luciferase values were normalized to the renilla luciferase control. Data shown are from one representative experiment done in triplicates (Student-t-Test).

e, Chromantin immunoprecipitation with anti-RIP140 (#ab42126) or IgG in MDA-MB-436. DNA bound DNA was amplified by qPCR with specific primers of the GLUT3 gene (SLC2A3).

f, Number of colonies of transformed MEF #1 stably expressing shGLUT3 and expressed as percent of WT shControl (shC) (n=2 independent experiments).

g, Cell proliferation measured by MTT assay of MEF #1 stably expressing an shRNA Control (shC) or a specific shRNA targeting *Glut3* (shGLUT3) and normalized by that of MEF WT at day 1 for each shRNA (representative experiment, Student-t-Test).

h, Cell viability assessed by crystal violet staining of MDA-MB-436 breast cancer cells after RIP140 siRNA silencing combined with siRNA GLUT3 (representative experiment, n=3

independent experiments). The proliferation of siRIP140 cells (siRIP) was expressed as relative to that of siControl cells (siC) for each conditions.

Fig. 5. RIP140 and p53 inhibit the expression of GLUT3 induced by HIF-2α.

a, Luciferase assay in MEF #1 WT transiently transfected with TK-Renilla, GLUT3-Luc reporter plasmids and increasing doses of p53 vector. Luciferase values were normalized to the renilla luciferase control. Data shown are from one representative experiment done in triplicates (Student-t-Test).

b, Luciferase assay in MEF #1 KO transiently transfected with TK-Renilla, GLUT3-Luc reporter plasmids, c-Myc-RIP140 and p53 vectors. Luciferase values were normalized to the renilla luciferase control. Data shown are from one representative experiment done in triplicates (Student-t-Test).

c, p53 protein level quantified by western blot in MEF#1. Unprocessed original scans of blots are shown in Supplementary Figure 7.

d, Luciferase assay in MEF #1 KO transiently transfected with TK-Renilla, GLUT3-Luc reporter plasmids and HA-HIF-1α or HA-HIF-2α vectors. Luciferase values were normalized

to the renilla luciferase control. Data shown are from one representative experiment done in triplicates (Student-t-Test).

e, HIF-1α and HIF-2α protein level quantified by western blot in MEF#1 in normoxia (21% O2). Unprocessed original scans of blots are shown in Supplementary Figure 7.

f, *GLUT3* mRNA level quantified by RT-qPCR in MEF #1 48h after HIF-2α silencing by siRNA(n=3 independent experiments).

g, Luciferase assay in MEF #1 transiently transfected with TK-Renilla, HRE-Luc reporter plasmids and increasing doses of c-myc-RIP140 vector. Luciferase values were normalized to the renilla luciferase control. Data shown are from one representative experiment done in triplicates (Student-t-Test).

h, Luciferase assay in MEF #1 KO transiently transfected with TK-Renilla, HRE-Luc reporter plasmids, HA-HIF-2α, c-myc-RIP140 (left panel) or p53 (right panel) expression plasmids. Luciferase values were normalized to the renilla luciferase control. Data shown are from one representative experiment done in triplicates (Student-t-Test).

i, Luciferase assay in MEF #1 KO transiently transfected with TK-Renilla, HRE-Luc reporter plasmids, HA-HIF-2α and p53 expression plasmids in combination with c-myc-RIP140 vector.

Luciferase values were normalized to the renilla luciferase control. Data shown are from one representative experiment done in triplicates (Student-t-Test).

j, Luciferase assay in MEF #1 KO transiently transfected with TK-Renilla, GLUT3-Luc reporter plasmids, HIF-2α and p53 expression plasmids in combination with c-myc-RIP140 vector. Luciferase values were normalized to the renilla luciferase control. Data shown are from one representative experiment done in triplicates (Student-t-Test).

k, Proximity ligation assay in MEF #1 WT between RIP140 and HIF-2α using rabbit anti-RIP140 and mouse anti-HIF-2α, between RIP140 and p53 using rabbit anti-RIP140 and mouse anti-p53 and between p53 and HIF-2α using mouse anti-p53 and rabbit anti-HIF-2α to detect endogenous proteins (left panel). Dots were quantified with the Duolink Software from 5 independent microscopic fields (right panel).

Fig. 6. The prognostic value of RIP140 is correlated with the levels of GLUT3 expression

Kaplan-Meier analysis plotting the survival curve of 1068 cases of breast cancer with statistical significance being assessed using the log-rank test from the TCGA dataset.

a, Kaplan-Meier curves showed worse overall survival rates for breast cancer patients with low RIP140 expression compared to patients with high RIP140 expression (P=0.042; left panel).

Kaplan-Meier curves showed worse overall survival rates for breast cancer patients with high GLUT3 (SLC2A3) expression compared to patients with low GLUT3 expression (P=0.01; right panel).

b, GLUT3 expression groups have been defined on the basis of the median GLUT3 expression. Kaplan-Meier curves showed better overall survival rates for breast cancer patients with high RIP140 expression in low GLUT3 expression group (P=0.0021; left panel). On the contrary, RIP140 prognostic value was not significant in high GLUT3 expression group (P=0.68).

c, Groups have been defined on the basis of the median p53 (TP53), HIF-2α (EPAS1) and HIF-1α (HIF1A) expression. RIP140 prognostic value was significant in high p53 (P=0.0081), low HIF-2α (P=0.0016) and low HIF-1α (P=0.015).

Fig. 7. Model: RIP140 inhibits tumorigenesis by affecting glycolysis through the blockade of GLUT3 expression. RIP140 and p53 cooperate to inhibit the expression of GLUT3 induced by HIF-α. Glycolysis-dependent proliferation of breast cancer cells is reduced, due to a decrease in glycolysis. The prognostic value of RIP140 is associated with good survival in patients with low GLUT3, high p53 and low HIF-α (right panel).

In patients with high HIF-α, low p53 and high GLUT3, RIP140 and p53 do not inhibit the transcriptional activity of HIF-α; GLUT3 is highly expressed and glycolysis is enhanced. In this sub-group, RIP140 expression level is not correlated with good survival.

Double blue lines represent cell membranes. The grey square represents GLUT3 gene, the grey ovoid forms represent GLUT3 protein. The orange circle represents glucose.

Supplementary Figure Legends

Supplementary Fig. 1. RIP140-deficiciency enhances cell proliferation and tumorigenesis.

a, RIP140 mRNA level quantified by RT-qPCR after silencing by two different siRNA specific of human RIP140 in MCF7 and MDA-MB436 breast cancer cells (n=4 independent experiments).

b, The slope of the curves was extracted using xCELLigence RTCA Software from the curves in Fig. 1a and 1b. The slopes of the curves were higher with siRIP140 than with control siRNA (siC).

c, MTT assay in MCF7 cells after RIP140 silencing by siRNA #2 (siRIP#2) (n=3 independent experiments).

d, Cell proliferation monitored by xCELLigence in MDA-MB-436 after RIP140 silencing by siRNA #2 (siRIP#2) (n=4 independent experiments).

e, The slope of the curves was extracted using xCELLigence RTCA Software from Supplementary 1d for MDA-MB-436 and from cell proliferation monitored by xCELLigence in DU145 and RKO after RIP140 silencing by siRNA #2 (siRIP#2) for 7 days.

f, RIP140 expression levels quantified by RT-qPCR (left panel; representative experiment; n= 4 experiments) and immunofluorescence (right panel) in the MEFs used in the study. MEF#1 were immortalized by the 3T3 protocol. MEF#2, #3 and #4 were transformed by the infection of SV40/H-RasV12 expressing retrovirus.

g, Cell proliferation of MEF #1 measured by MTT assay (n=4 independent experiments).

h, ATP level in MEF #1 relative to WT (n=3 independent experiments).

i, MTT assay in SV40/H-RasV12-transformed RIP140 WT and KO MEF #3 (representative experiment, n=3 independent experiments).

j, Number of colonies from soft agar assay of MEF #2 and #3 (n=3 independent experiments).

k, Human RIP140 mRNA level quantified by RT-qPCR in MEF #1 stably overexpressing a pEGFP plasmid (WT+GFP) and (RIPKO+GFP) or a pEGFP-hRIP140 plasmid

(RIPKO+hRIP140). Primers used are specific for the human RIP140 sequence (representative experiment, n=4 independent experiments).

l, Relative MTT assay at day 6 of MEF #1 overexpressing GFP or GFP-hRIP140 (n=3 independent experiments).

m, Representative pictures of colony soft agar assays of MEF #1 quantified in Fig. 1h.

n, Pictures of xenografted nude mice with MEF #2 from Fig. 1e.

o, Tumor growth curve of H-RasV12-MEF #1 xenografted in nude mice (n=6).

Supplementary Fig. 2. Inhibiting glycolysis reduces the growth advantage of RIP140-deficient cells.

Unless otherwise stated, MEF #1 were used.

a, Representative pictures of MEF #1 under glucose starvation.

b, MTT assay at day 10 represented in Fig. 2a. RIPKO cell proliferation was expressed as relative to that of WT cells in presence of glucose (4.5g/L).

c, MTT assay of transformed MEF #3 following glucose deprivation for 4 days and represented as percent of Glucose 4.5g/L for each cell line (n=3 independent experiments).

d, Cell proliferation analyzed by MTT assay upon 2-deoxyglucose treatment (2DG; 5mM) (n=3 independent experiments).

e, MTT assay of MEF #3 upon BrP treatment (100µM) (representative experiment, n=3 independent experiments).

f, Relative cell index is represented as percent of control after four days of 2DG treatment (5mM)(representative experiments, n=2; Student-t-test).

g, Crystal violet staining of MEF #3 after 3 weeks of 2-DG (5mM) treatment. This shows that RIPKO colonies were more numerous than WT colonies and that 2DG treatment abolished the growth of RIPKO colonies.

h, Cell viability assessed by crystal violet staining of MDA-MB-436 after RIP140 silencing by siRNA at day seven and represented as percent of control after BrP (100µM) treatment (n=3 independent experiments).

Supplementary Fig. 3. RIP140-deficiency enhances glycolysis in cancer cells.

a, Glycolysis represented as relative ECAR normalized to protein quantity in MEF #3 (representative experiment, n=3 independent experiments.

b, Extracellular acidification rate (ECAR) normalized by protein content in MDA-MB-436 after siRNA silencing of RIP140 (siRIP#2) for 48h (representative experiment, n=3 independent experiments).

c, Glycolysis represented as relative ECAR measured by Seahorse Bioscience Flux Analyzer and normalized to protein quantity in colon (RKO) and prostate cancer cell lines (DU145, PC3) after RIP140 silencing by siRNA (siRIP#2)(representative experiment, n=2 independent experiments).

Supplementary Fig. 4. GLUT3 and G6PD are essential for the growth advantage induced by RIP140-deficiency.

a, Gene expression level quantified by RT-qPCR of glycolytic genes in MEF #1 obtained from three independent samples. Data are expressed as relative to MEF WT.

b, *Glut3* mRNA levels quantified by RT-qPCR in MEF #3 (n=3 independent experiments).

c, mRNA level of *RIP140* quantified by RT-qPCR in MCF7 after RIP140 silencing by two different specific siRNA (n=3 independent experiments).

d, Protein expression level of GLUT3 and Actin quantified by western blot in MEF #1. Unprocessed original scans of blots are shown in Supplementary Figure 7.

e, Knockdown efficiency of *Glut3* by specific shRNA was determined by western blot (left panel) and RT-qPCR (right panel) (n=3 independent experiments).

f, siRNA efficiency was verified by RT-qPCR for *RIP140* (left panel) and *GLUT3* (right panel) 48h after transfection in MDA-MD-436.

Supplementary Fig. 5. RIP140 and p53 inhibit the expression of GLUT3 induced by HIF-2α.

a, p53, HIF-1α and HIF-2α mRNA level quantified by RT-qPCR in MEF #1 and #3 (n=3 independent).

b, HIF-2α mRNA level quantified by RT-qPCR in MEF #1 after siRNA silencing (n=3 independent experiments).

c, Luciferase assay in MEF #1 KO transiently transfected with TK-Renilla, HRE-Luc reporter plasmids, HA-HIF-1α, c-myc-RIP140 (left panel) or p53 (right panel) expression plasmids. Luciferase values were normalized to the renilla luciferase control. Data shown are from one representative experiment done in triplicates (Student-t-Test).

d, Luciferase assay in MEF #1 WT transiently transfected with TK-Renilla, HRE-Luc reporter plasmids, HA-HIF-1α and p53 expression plasmids in combination with c-myc-RIP140 vector.

Luciferase values were normalized to the renilla luciferase control. Data shown are from one representative experiment done in triplicates (Student-t-Test).

Supplementary Fig. 6. The prognostic value of RIP140 is correlated with the levels of GLUT3 expression

Kaplan-Meier of 1068 cases of breast cancer with statistical significance being assessed using the log-rank test from the TCGA dataset.

a, Groups have been defined on the basis of the median p53 (TP53, top panel), HIF-2α (EPAS1, middle panel) and HIF-1α (HIF1A, bottom panel) expression. Kaplan-Meier analyses plotting the survival curved used to define RIP140 prognostic value in Fig. 6c.

b, GLUT3 expression groups have been defined on the basis of the median GLUT3 expression for colon and stomach cancer patients. RIP140 prognostic value was significantly associated with better overall survival in low GLUT3 expression group (colon, P=0.048; stomach, P=0.022).

Supplementary Fig. 7. Unprocessed original scans of blots.

Unprocessed images of all Western blots as indicated. Molecular size markers in kDa.

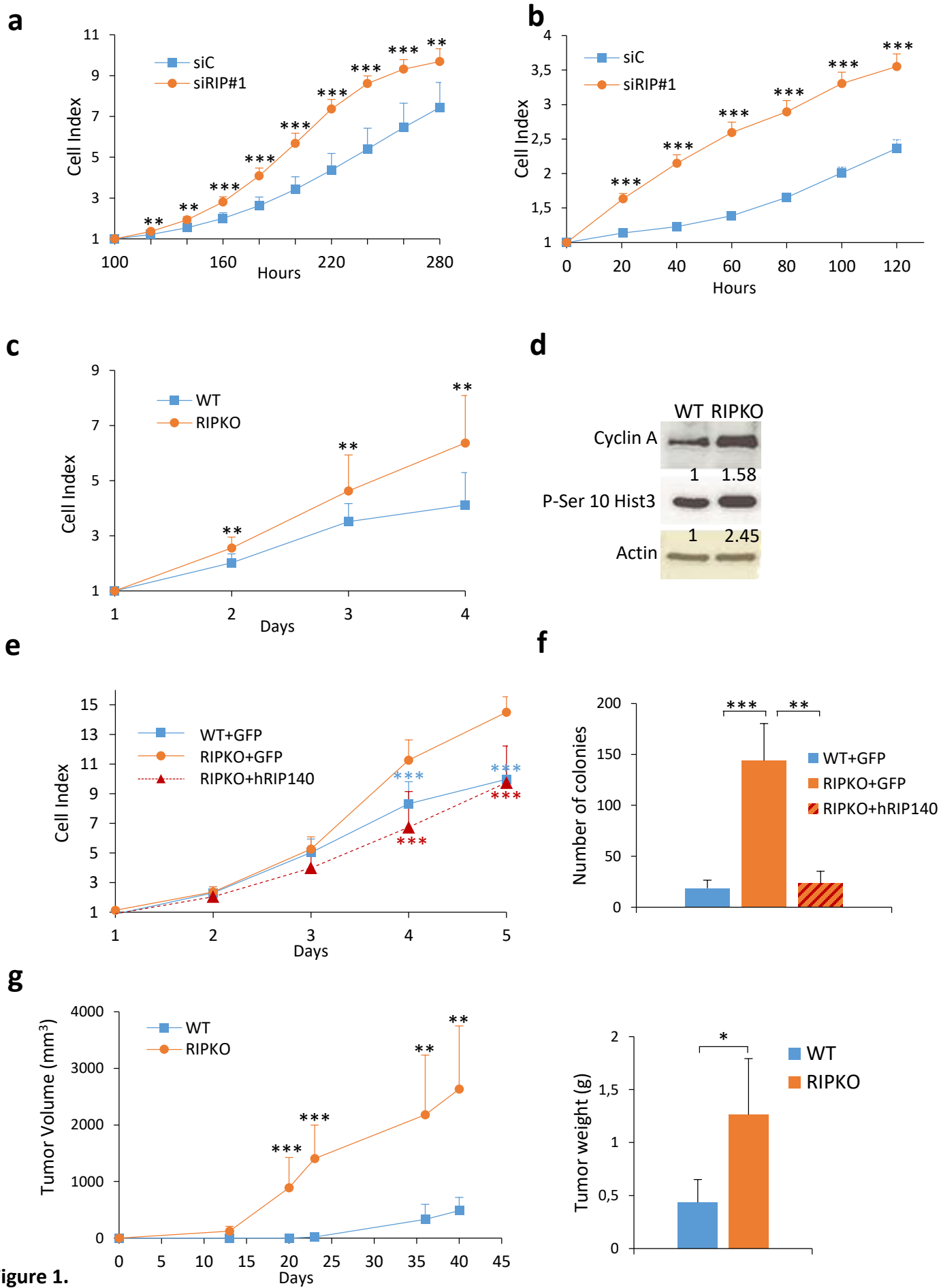
a
Cell Index
Hours
siC
siRIP#1
b
Cell Index
Hours
siC
siRIP#1
c
Cell Index
Days
WT
RIPKO
d
WT RIPKO
Cyclin A
1 1.58
P-Ser 10 Hist3
1 2.45
Actin
e
Cell Index
Days
WT+GFP
RIPKO+GFP
RIPKO+hRIP140
f
Number of colonies
WT+GFP
RIPKO+GFP
RIPKO+hRIP140
g
Tumor Volume (mm³)
Days
WT
RIPKO
Tumor weight (g)
WT
RIPKO

Figure 1.

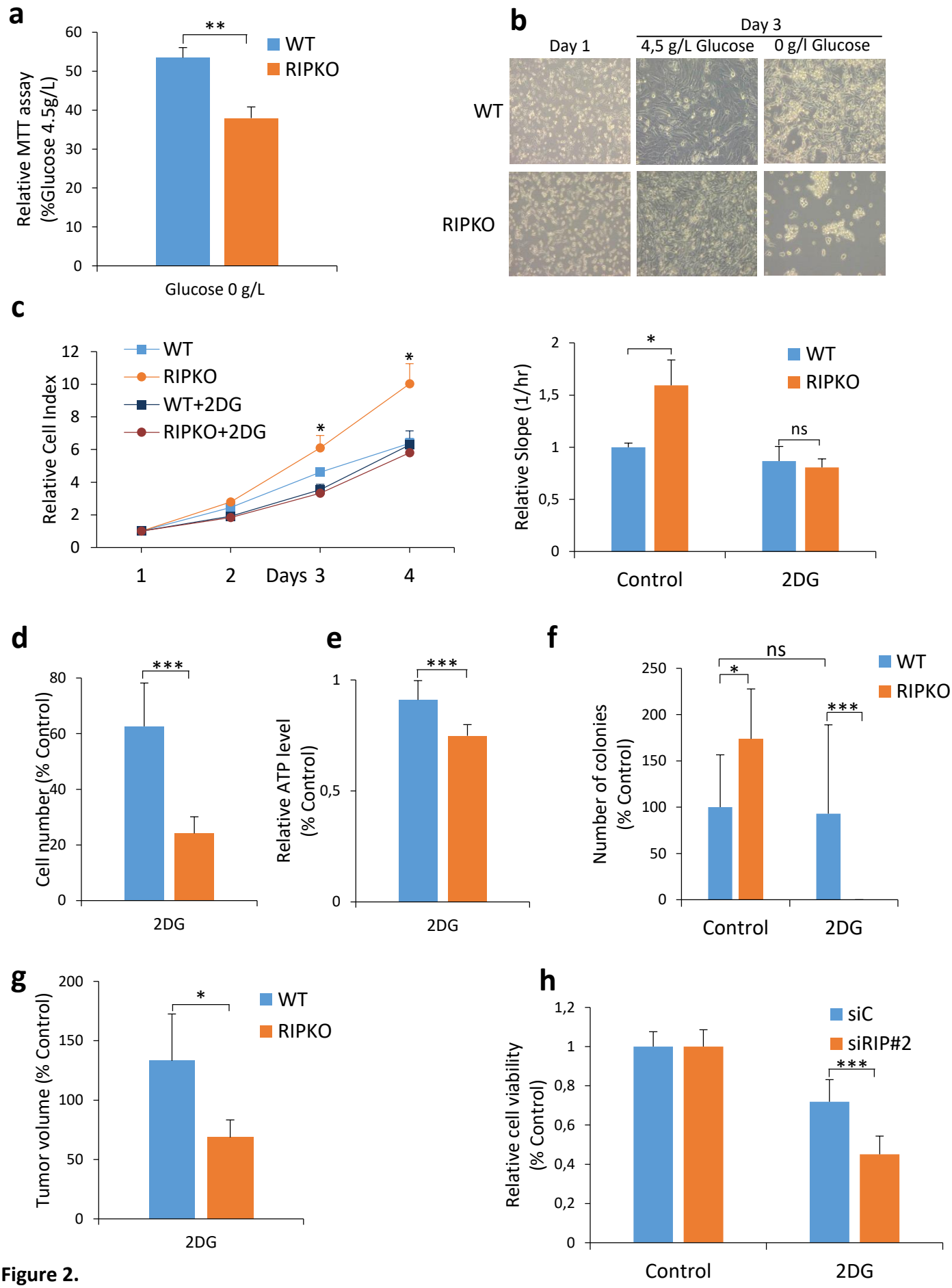
a
Relative MTT assay (%Glucose 4.5g/L)
60
50
40
30
20
10
0
**
WT
RIPKO
Glucose 0 g/L
b
Day 1
Day 3
4,5 g/L Glucose
0 g/l Glucose
WT
RIPKO
c
Relative Cell Index
12
10
8
6
4
2
0
WT
RIPKO
WT+2DG
RIPKO+2DG
*
*
1
2
Days 3
4
Relative Slope (1/hr)
2
1,5
1
0,5
0
*
ns
WT
RIPKO
Control
2DG
d
Cell number (% Control)
80
60
40
20
0
***
2DG
e
Relative ATP level (% Control)
1
0,5
0
***
2DG
f
Number of colonies (% Control)
250
200
150
100
50
0
ns
*
***
WT
RIPKO
Control
2DG
g
Tumor volume (% Control)
200
150
100
50
0
*
WT
RIPKO
2DG
h
Relative cell viability (% Control)
1,2
1
0,8
0,6
0,4
0,2
0
siC
siRIP#2
***
Control
2DG

Figure 2.

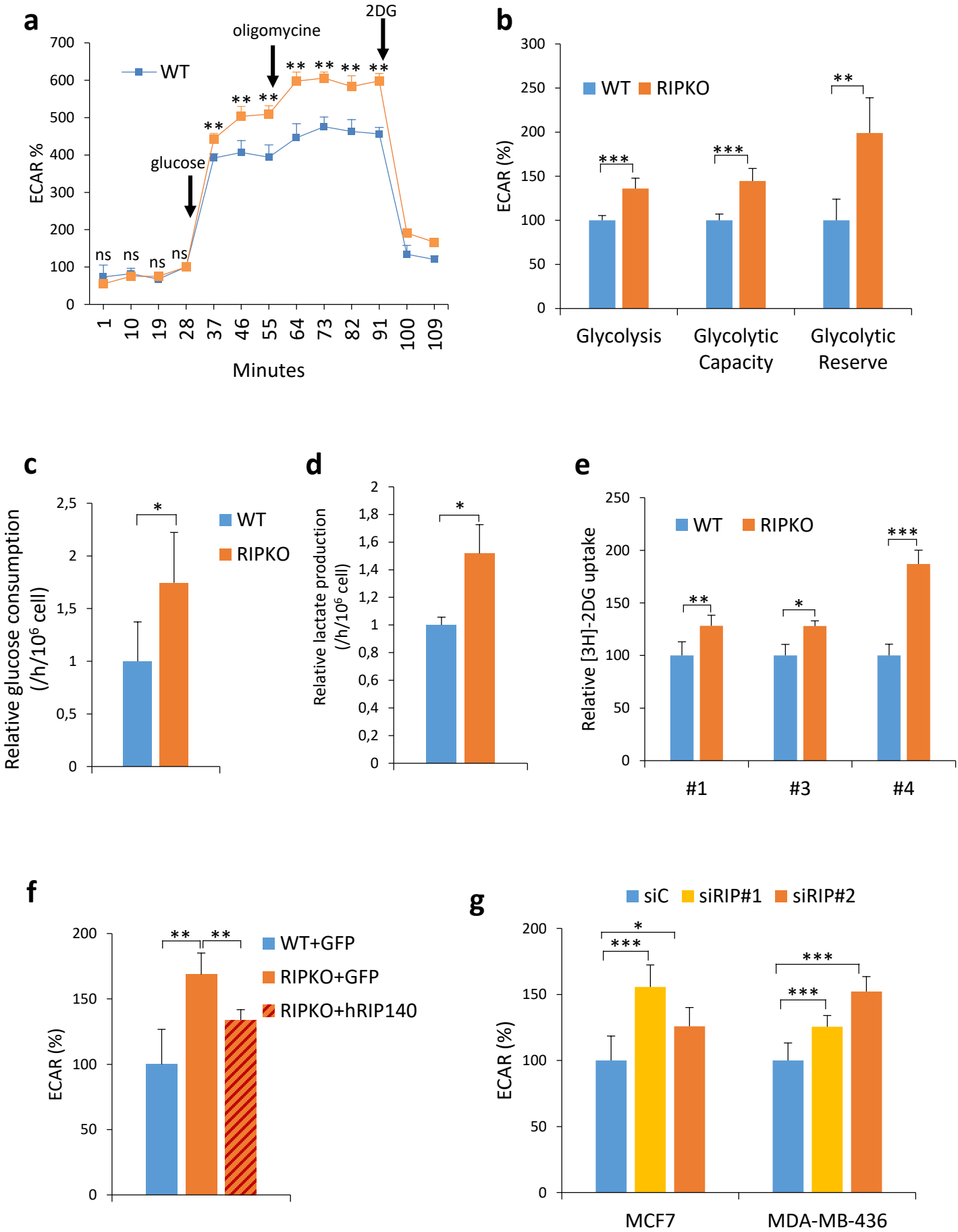
a
oligomycine
2DG
glucose
WT
ECAR %
Minutes
b
WT
RIPKO
ECAR (%)
Glycolysis
Glycolytic Capacity
Glycolytic Reserve
c
WT
RIPKO
Relative glucose consumption (/h/10⁶ cell)
d
Relative lactate production (/h/10⁶ cell)
e
WT
RIPKO
Relative [3H]-2DG uptake
#1
#3
#4
f
WT+GFP
RIPKO+GFP
RIPKO+hRIP140
ECAR (%)
g
siC
siRIP#1
siRIP#2
ECAR (%)
MCF7
MDA-MB-436

Figure 3.

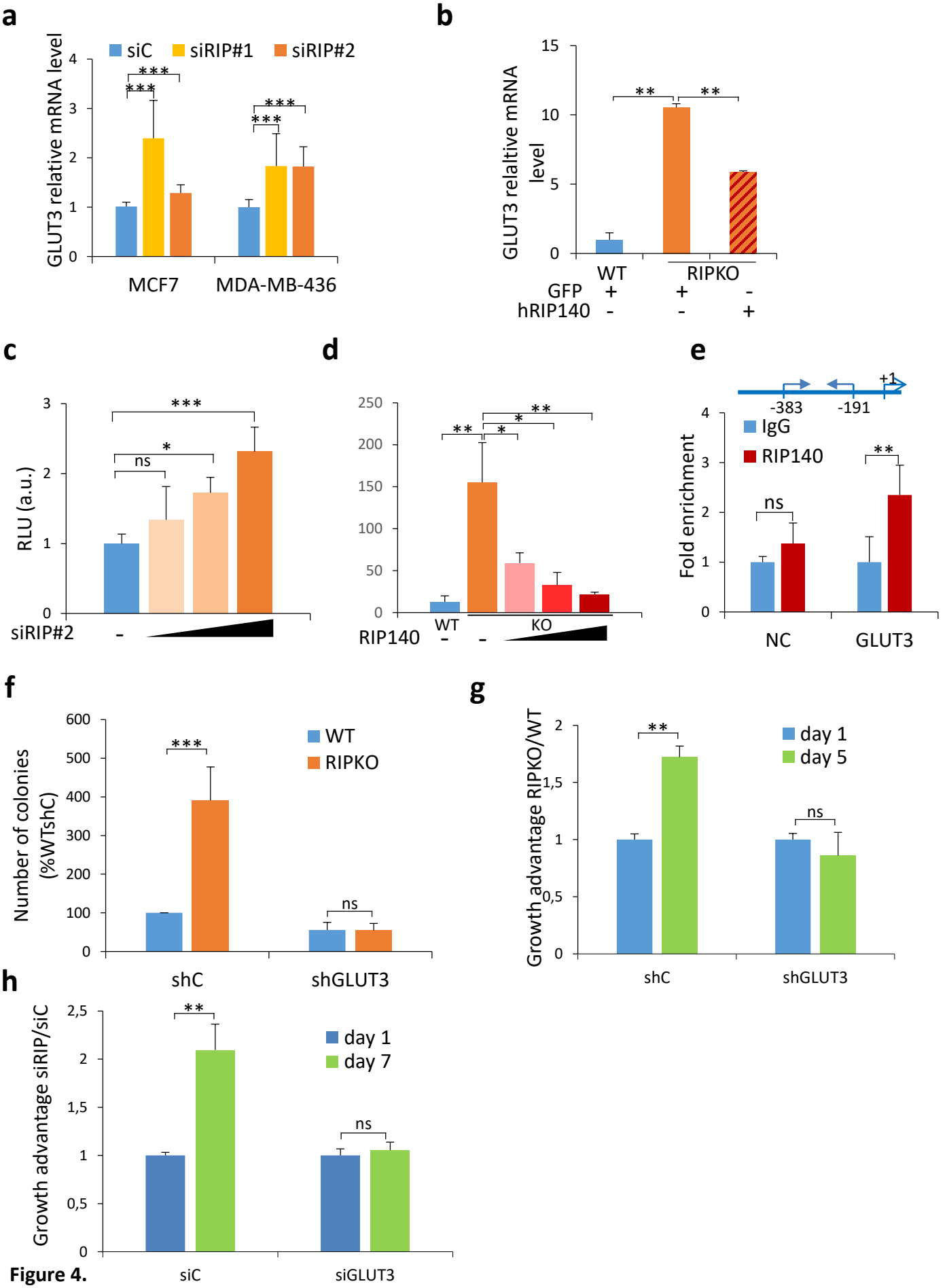
a
siC
siRIP#1
siRIP#2
GLUT3 relative mRNA level
MCF7
MDA-MB-436
b
GLUT3 relative mRNA level
WT
RIPKO
GFP
hRIP140
c
RLU (a.u.)
siRIP#2
d
RIP140
WT
KO
e
-383
-191
+1
IgG
RIP140
Fold enrichment
NC
GLUT3
f
Number of colonies (%WTshC)
WT
RIPKO
shC
shGLUT3
g
Growth advantage RIPKO/WT
day 1
day 5
shC
shGLUT3
h
Growth advantage siRIP/siC
day 1
day 7
siC
siGLUT3

Figure 4.

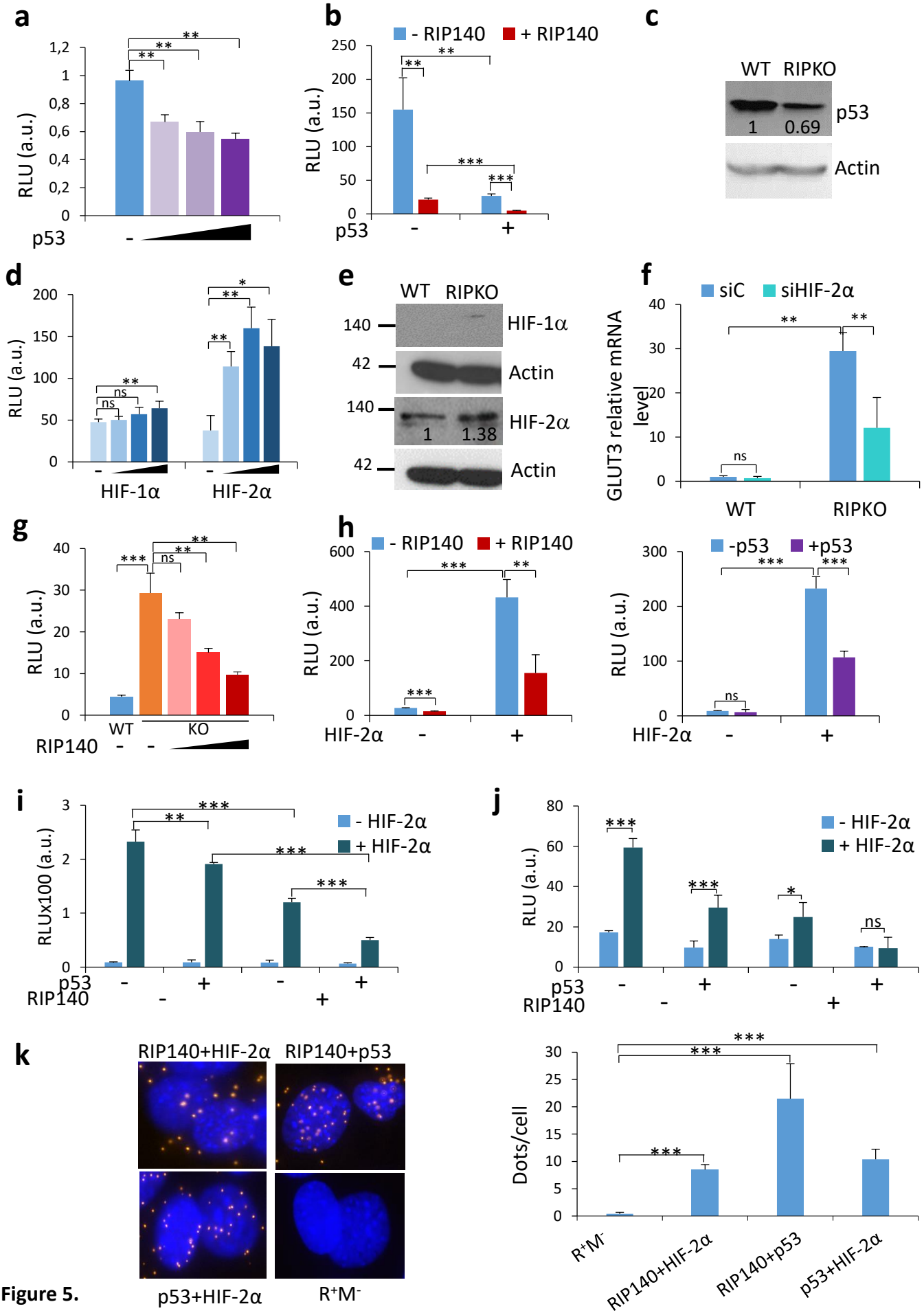
a
RLU (a.u.)
p53
b
- RIP140
+ RIP140
RLU (a.u.)
p53
c
WT
RIPKO
p53
1
0.69
Actin
d
RLU (a.u.)
HIF-1α
HIF-2α
e
WT
RIPKO
HIF-1α
Actin
HIF-2α
Actin
1
1.38
f
siC
siHIF-2α
GLUT3 relative mRNA level
WT
RIPKO
g
RLU (a.u.)
WT
KO
RIP140
h
- RIP140
+ RIP140
RLU (a.u.)
HIF-2α
-p53
+p53
RLU (a.u.)
HIF-2α
i
RLUx100 (a.u.)
- HIF-2α
+ HIF-2α
p53
RIP140
j
RLU (a.u.)
- HIF-2α
+ HIF-2α
p53
RIP140
k
RIP140+HIF-2α
RIP140+p53
p53+HIF-2α
R+M-
Dots/cell
R+M-
RIP140+HIF-2α
RIP140+p53
p53+HIF-2α

Figure 5.

a

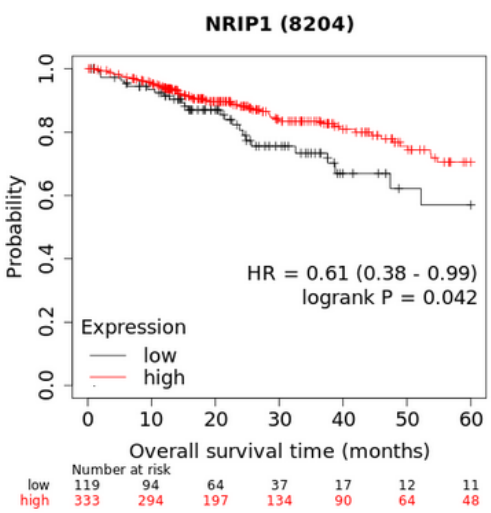

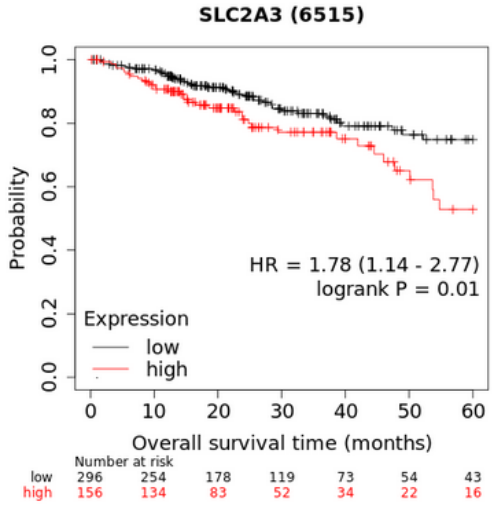

b

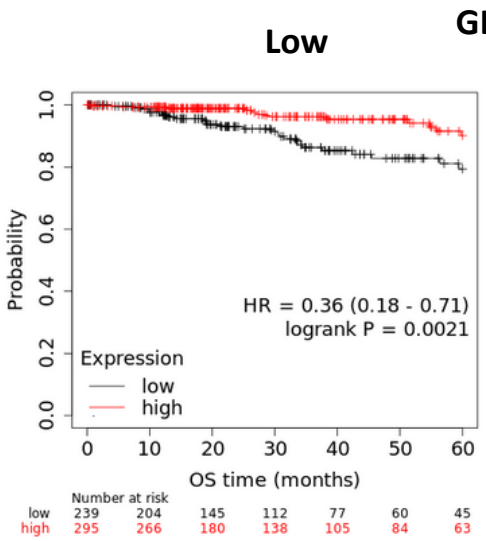

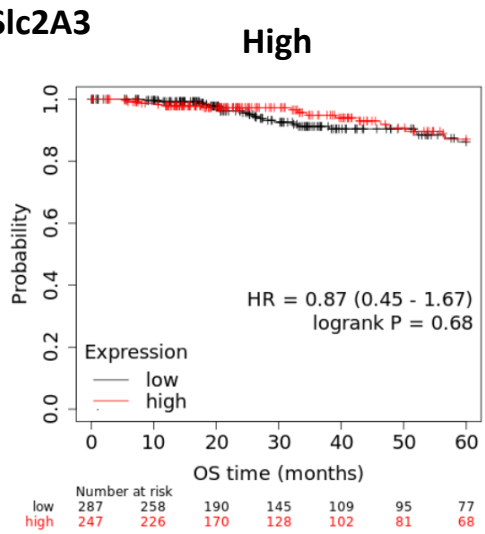

c

Tumor type	Nb of patients	Gene	Subgroup	NRIP1 cut-off	Nb of patients Low NRIP1	Nb of patients High NRIP1	HR	CI	p value
Breast	1068	SLC2A3	Low	2247	239	295	0.36	0.18 - 0.71	0.0021*
			High	2247	287	247	0.87	0.45 - 1.67	0.68
		TP53	Low	1991	210	323	0.79	0.17 - 0.86	0.48
			High	1991	251	282	0.41	0.38 - 1.19	0.0081*
		EPAS1	Low	2088	257	277	0.34	0.17 - 0.69	0.0016*
			High	2088	227	307	0.85	0.44 - 1.64	0.63
		HIF1A	Low	2083	218	316	0.38	0.17 - 0.86	0.015*
			High	2083	263	271	0.68	0.38 - 1.19	0.17

Figure 6.

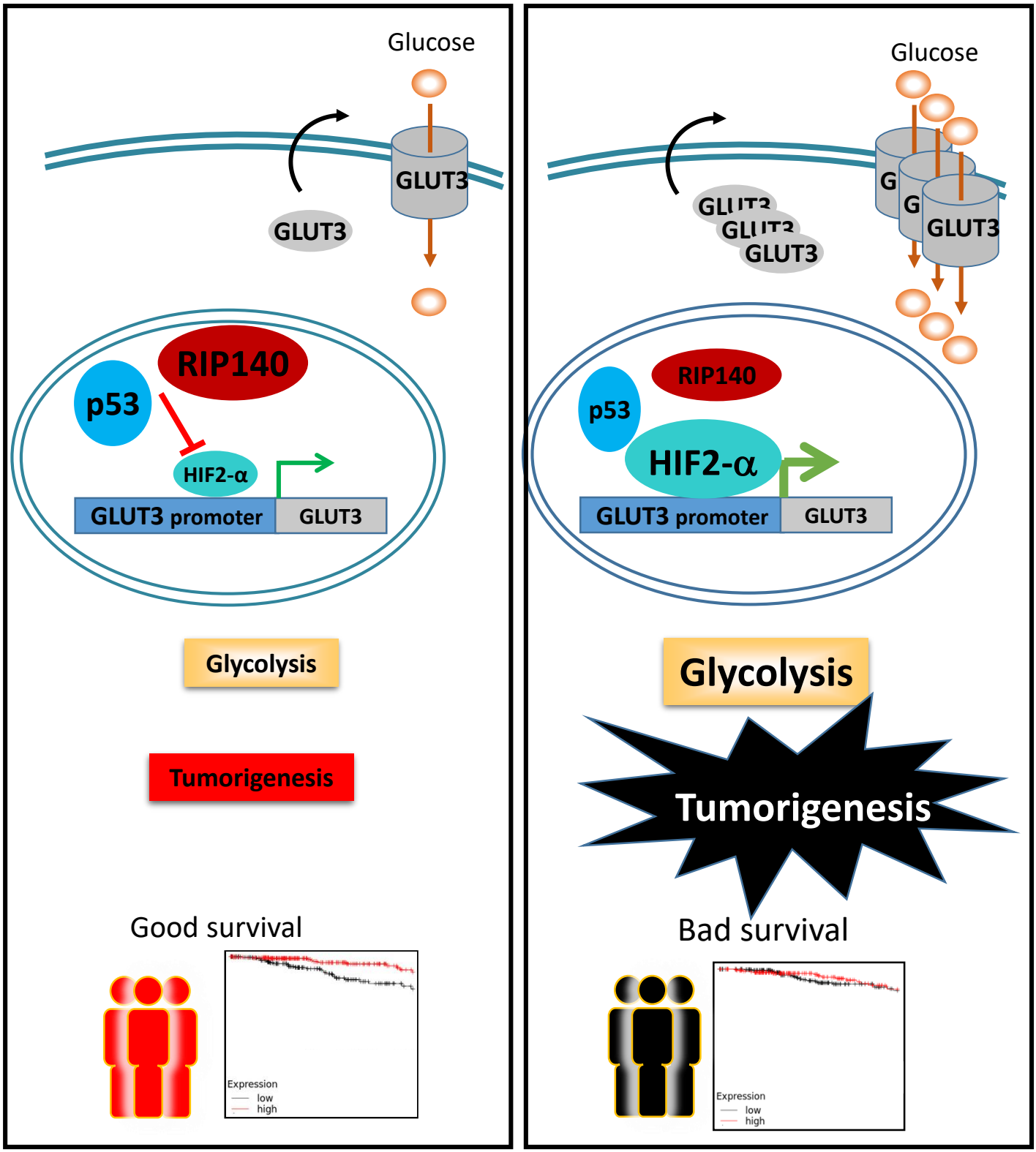
Glucose
GLUT3
GLUT3
RIP140
p53
HIF2-α
GLUT3 promoter
GLUT3
Glycolysis
Tumorigenesis
Good survival
Expression
low
high
Glucose
GLUT3
GLUT3
GLUT3
RIP140
p53
HIF2-α
GLUT3 promoter
GLUT3
Glycolysis
Tumorigenesis
Bad survival
Expression
low
high

Figure 7.

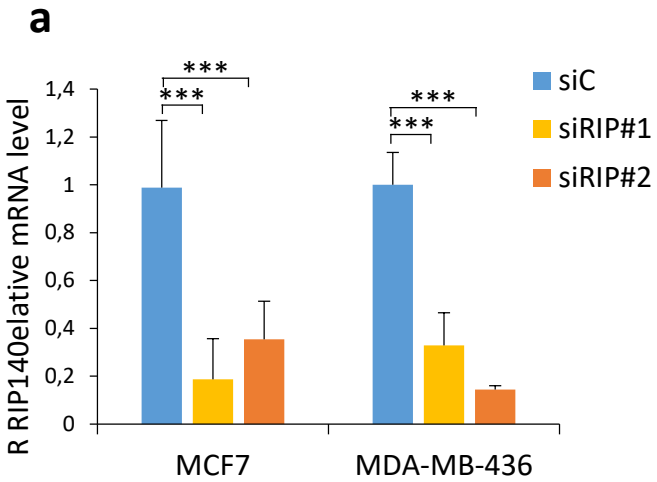

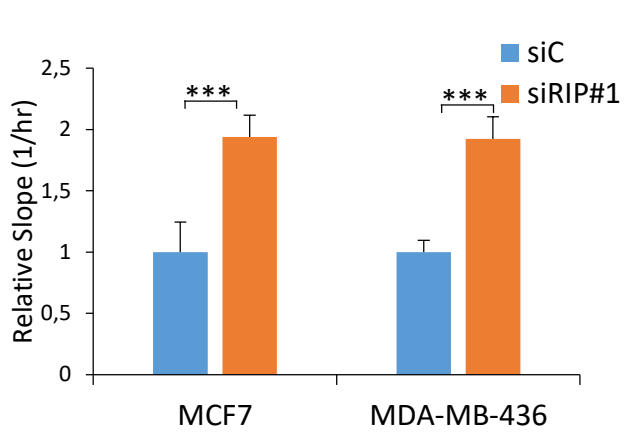

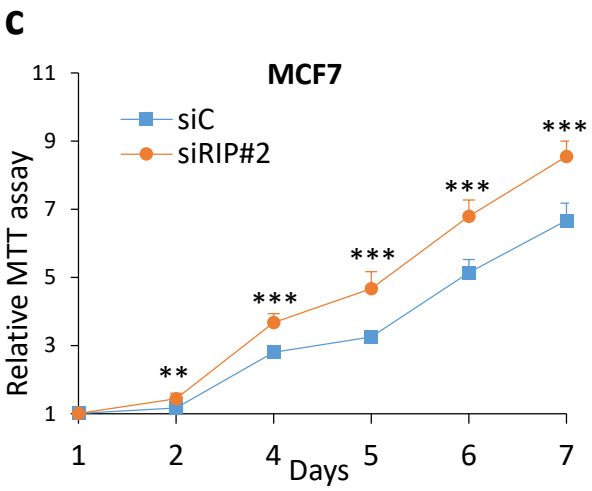

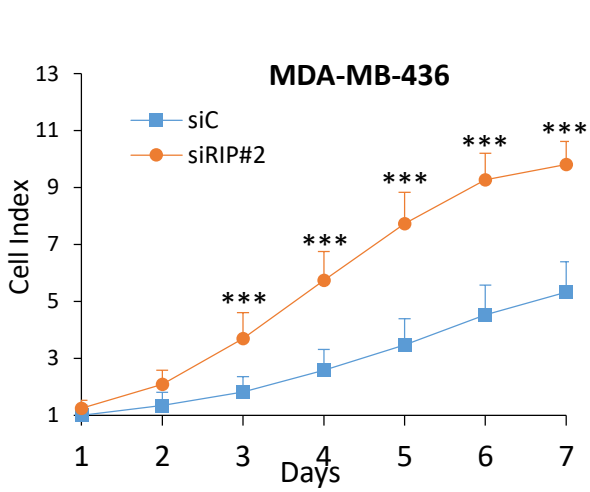

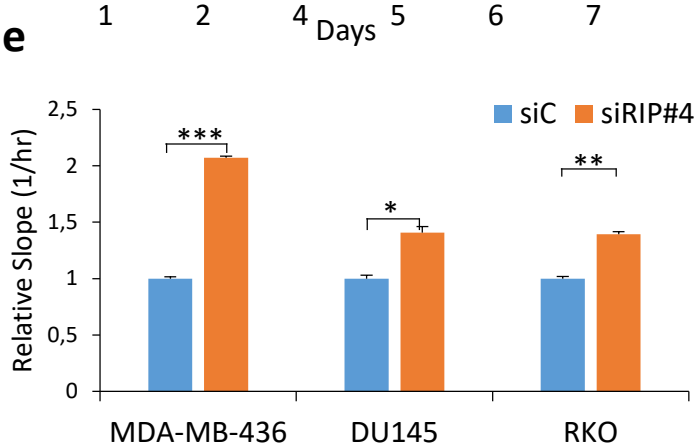

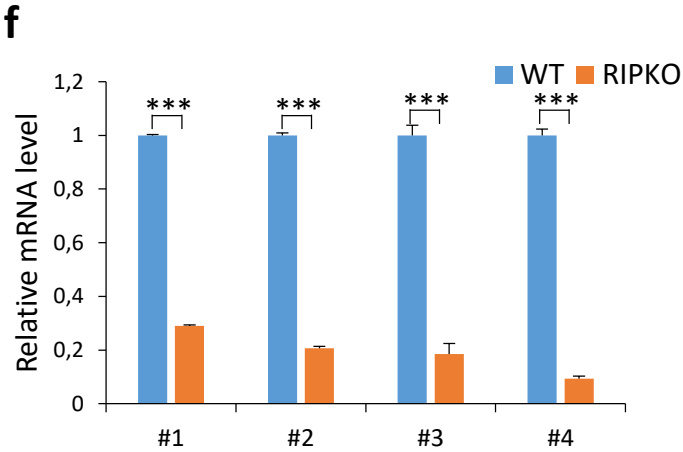

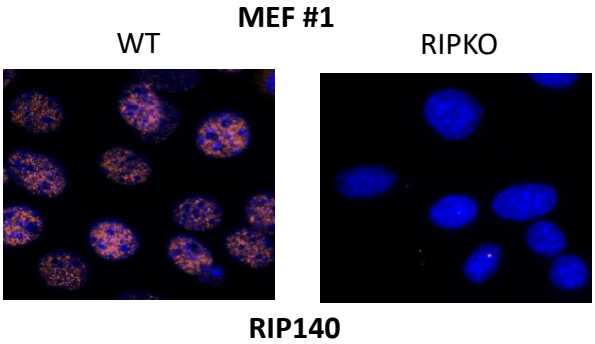

Supplementary Figure 1.

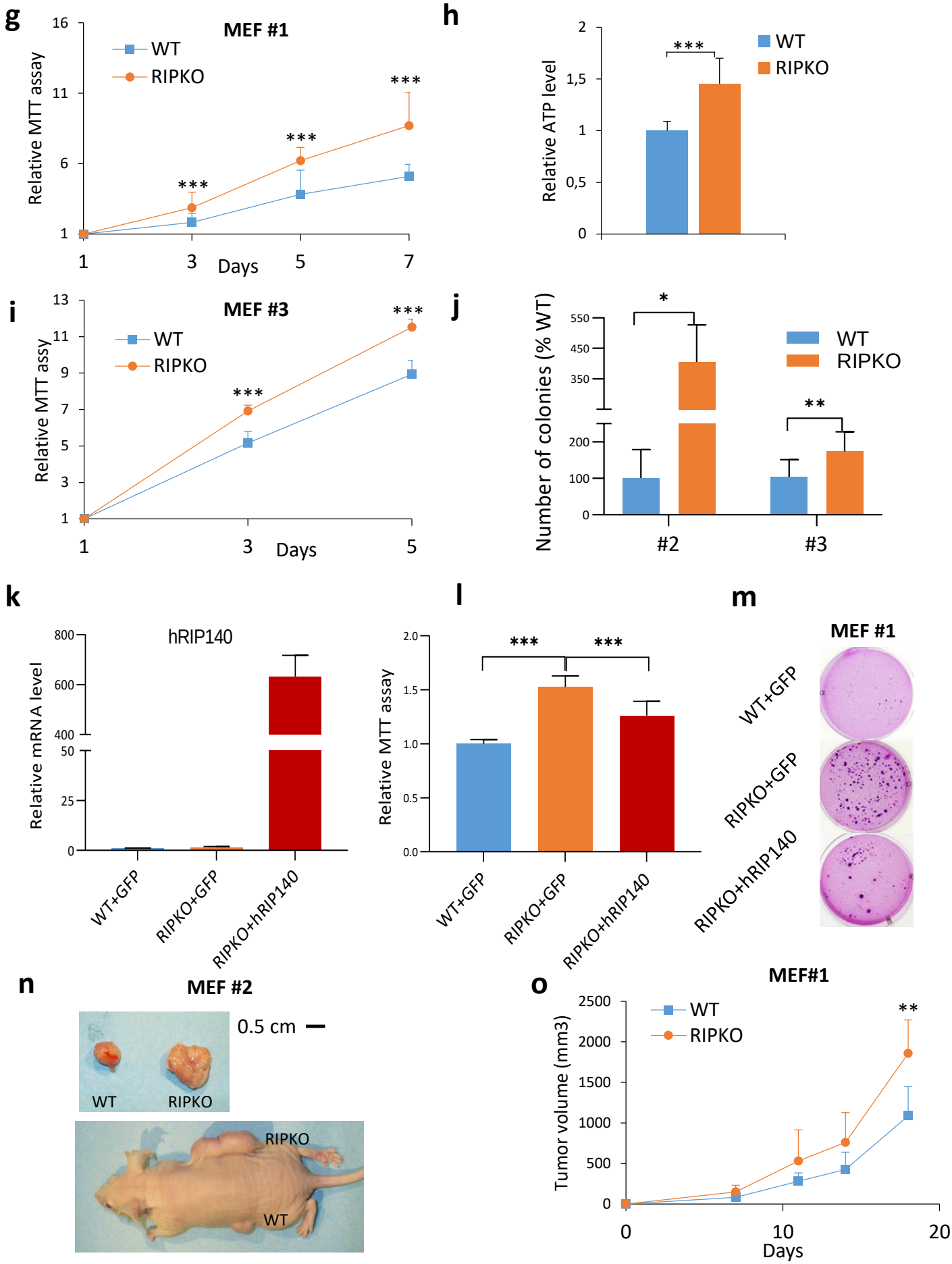

Supplementary Figure 1.

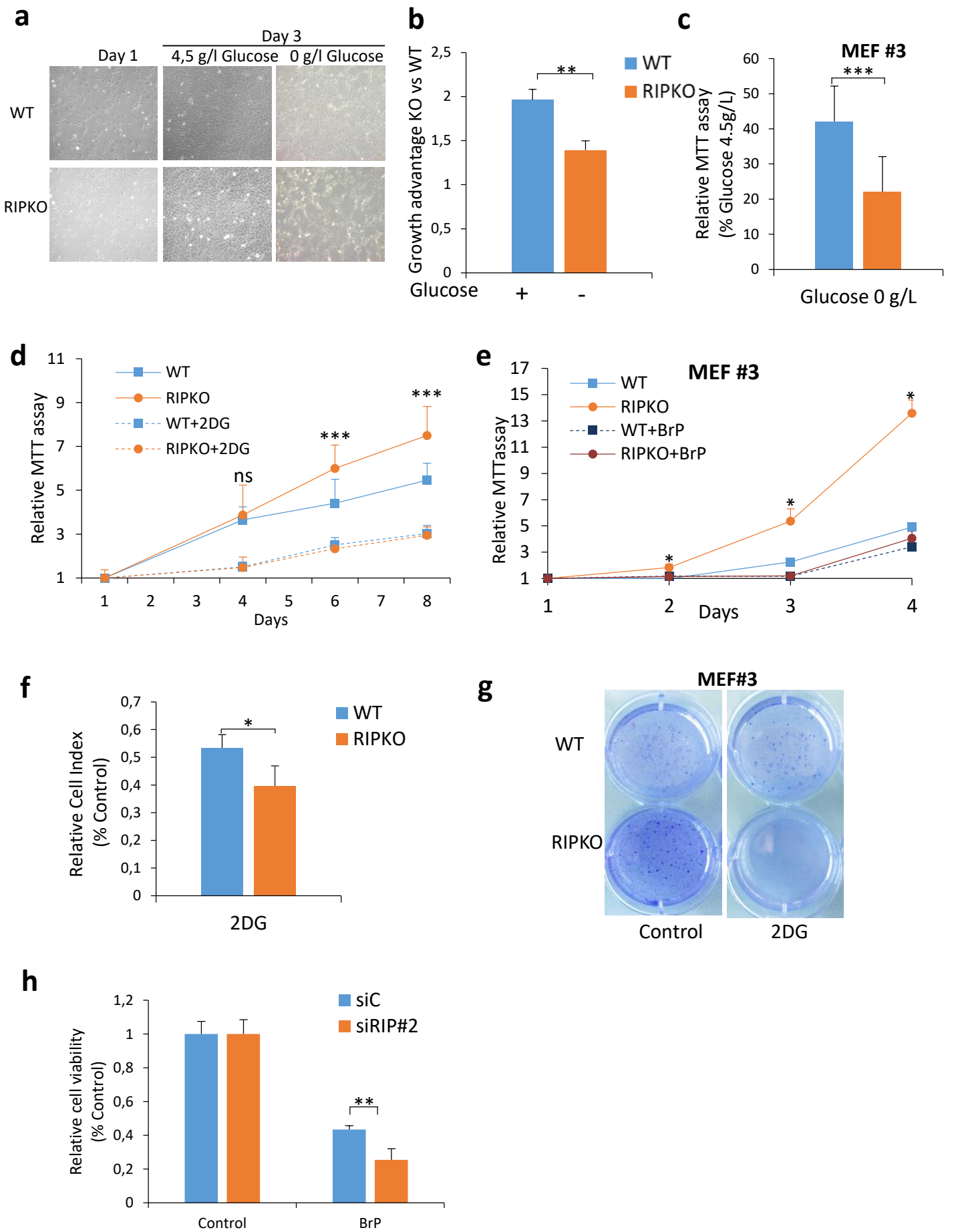

Supplementary Figure 2.

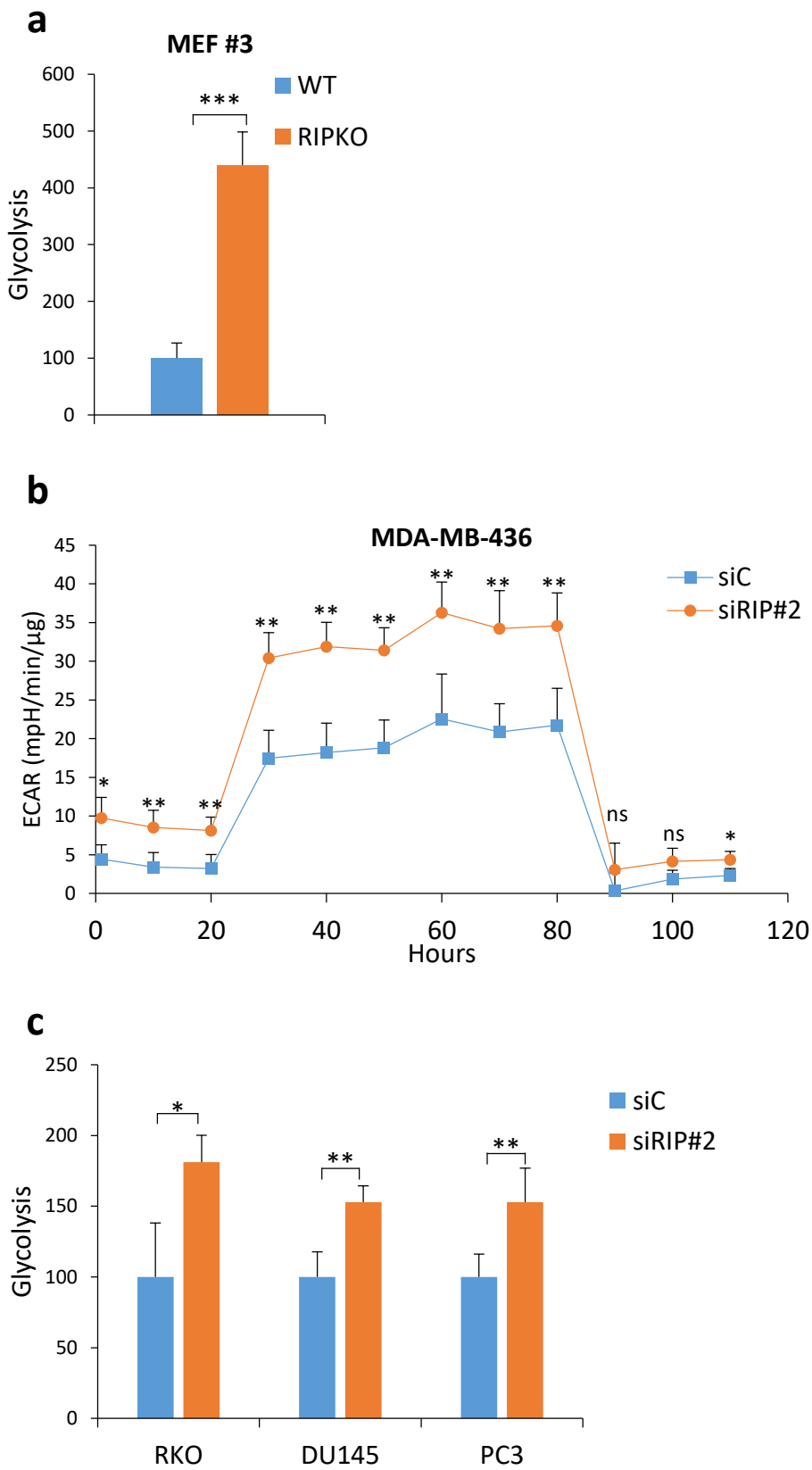

Supplementary Figure 3.

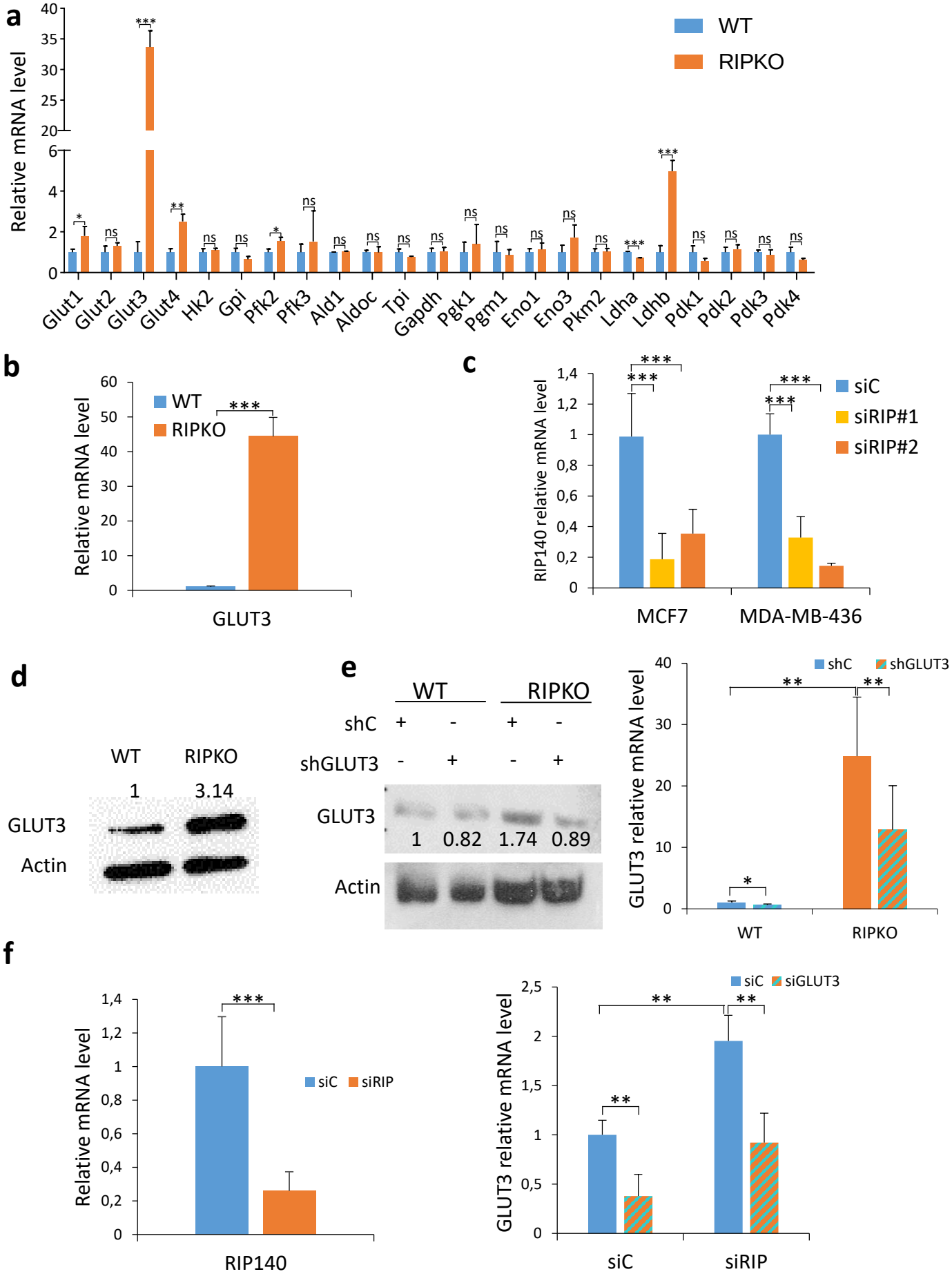

Supplementary Figure 4.

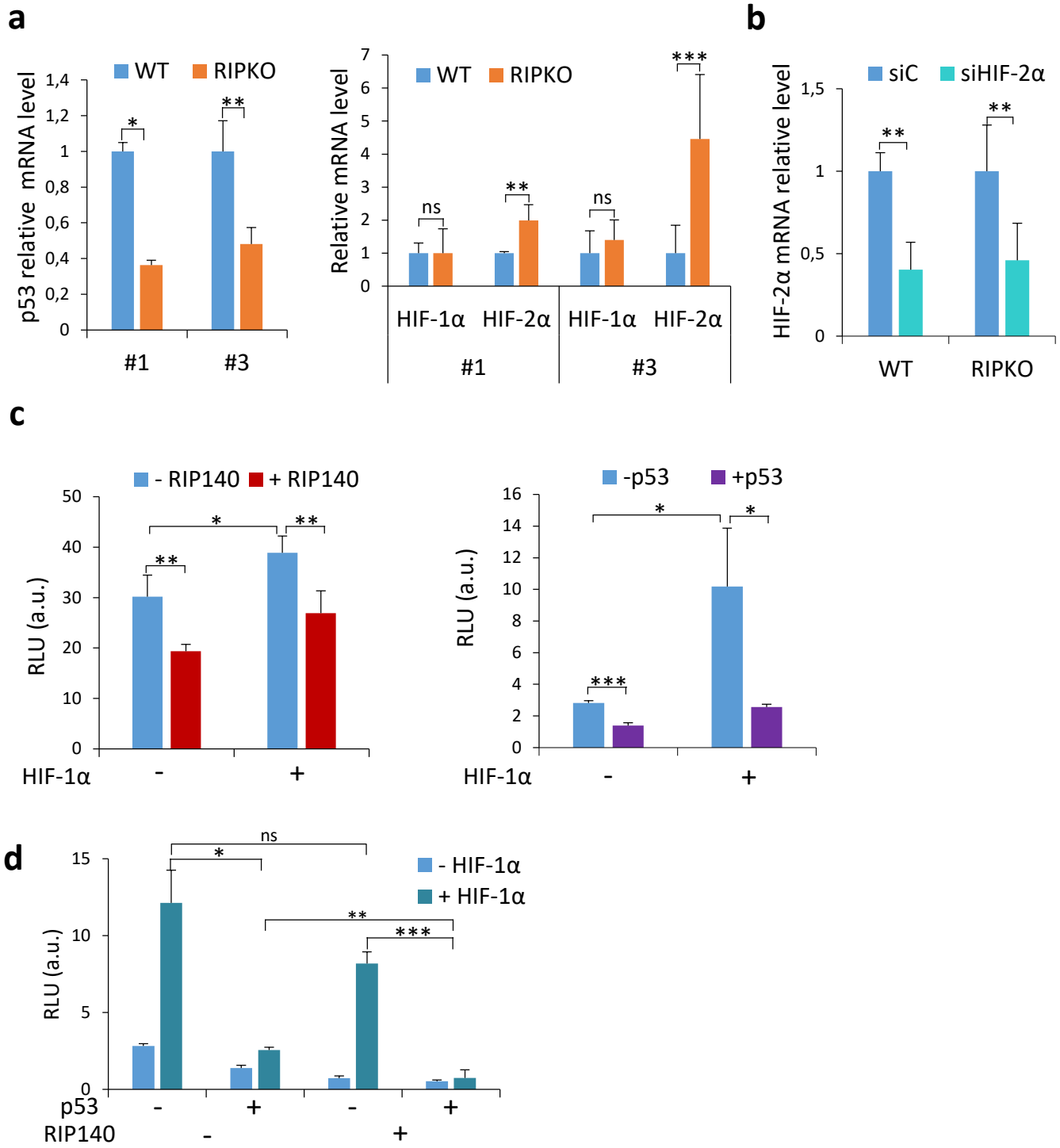

Supplementary Figure 5.

a

Low **High**

TP53

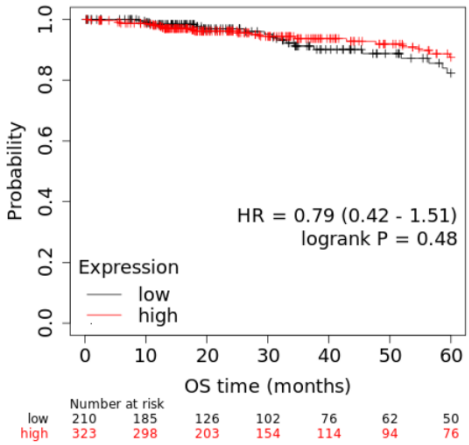

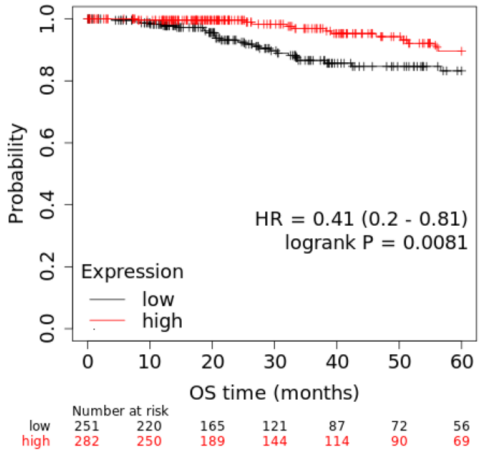

HIF-2α/EPAS1

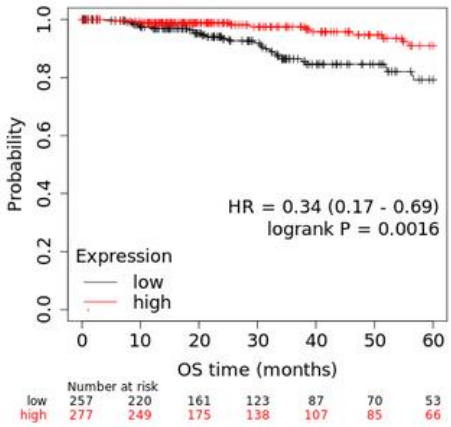

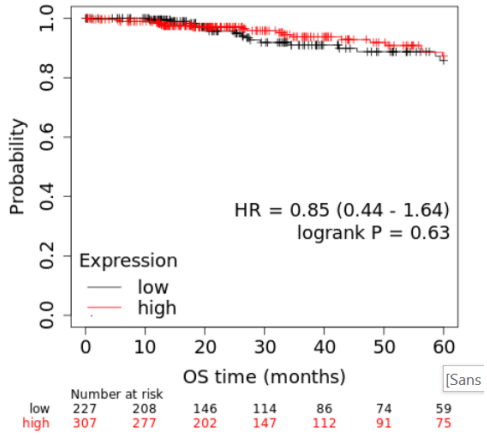

HIF-1α

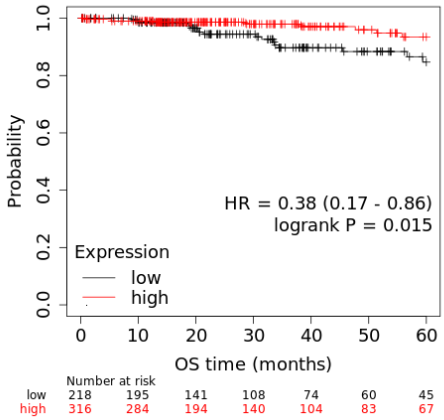

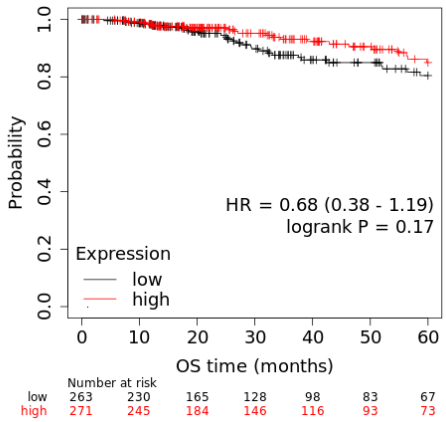

b

Tumor type	Nb of patients	Gene	Subgroup	NRIP1 cut-off	Nb of patients Low NRIP1	Nb of patients High NRIP1	HR	CI	p value
Colon	**450**	SLC2A3	Low	931	102	123	0.49	0.24 - 1.01	0.048*
			High	931	82	143	1.16	0.63 - 2.16	0.63
Stomach	**388**	SLC2A3	Low	1194	100	94	0.54	0.31 - 0.92	0.022*
			High	1194	80	114	1.15	0.76 - 1.74	0.51

Supplementary Figure 6.

Related to Fig. 1d

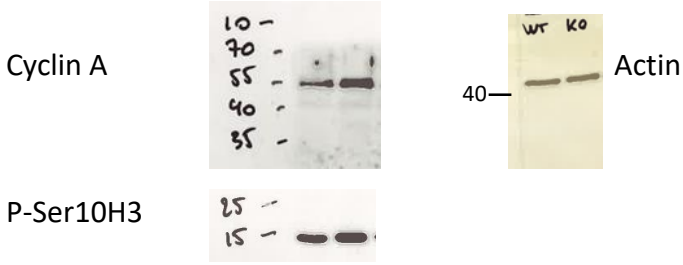

Related to Supplementary Fig. 4d

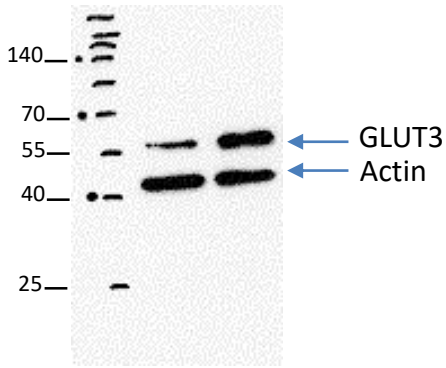

Related to Supplementary Fig. 4e

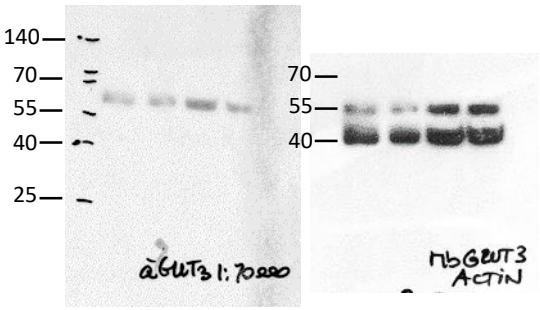

Supplementary Figure 7.

Related to Supplementary Fig. 5c

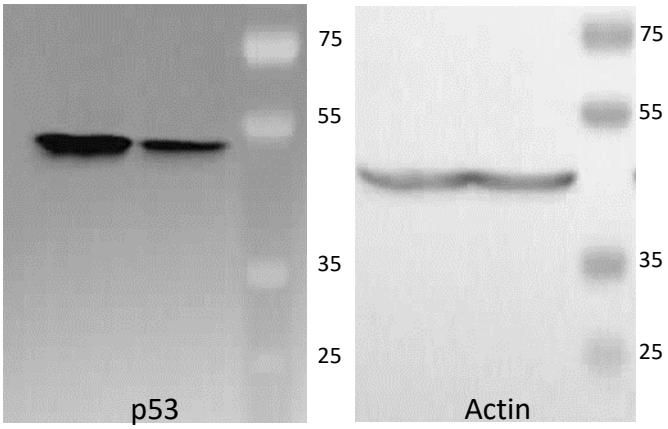

Related to Supplementary Fig. 5e

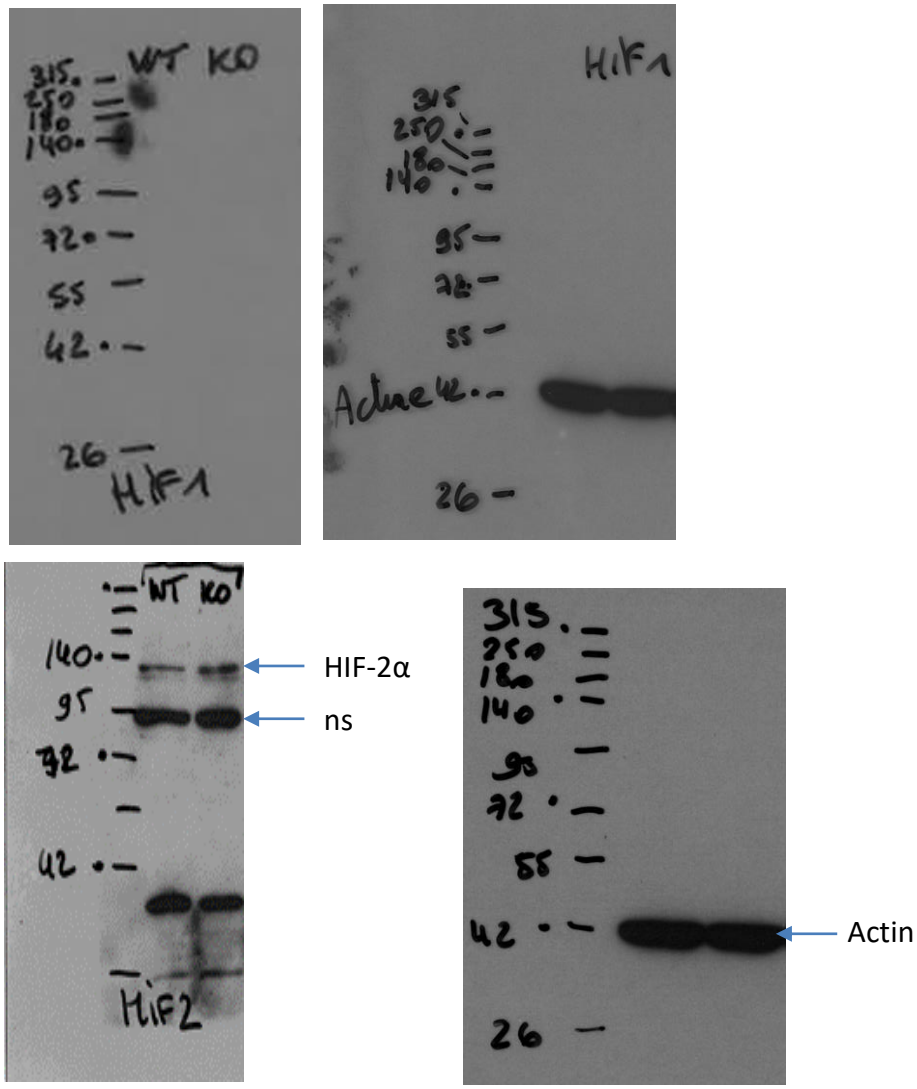

Supplementary Figure 7.